Current Zoology, 2023, **69**, 456–474
https://doi.org/10.1093/cz/zoac055
Advance access publication 16 July 2022
Original Article

Multivariate analyses of skull morphology inform the taxonomy and evolution of geomyoid rodents

Lily A. Noftz[a] and Jonathan J.M. Calede[a,b,*]

[a]Biology Program, The Ohio State University at Marion, 1459 Mount Vernon Avenue, Marion, OH 43302, USA, and
[b] Department of Evolution, Ecology, and Organismal Biology, The Ohio State University, 318 W. 12th Ave., Columbus, OH 43210, USA.

[*]Address correspondence to Jonathan J.M. Calede. E-mail: calede.1@osu.edu
Handling editor: Zhi-Yun JIA

Abstract

Morphological analyses are critical to quantify phenotypic variation, identify taxa, inform phylogenetic relationships, and shed light on evolutionary patterns. This work is particularly important in groups that display great morphological disparity. Such is the case in geomyoid rodents, a group that includes 2 of the most species-rich families of rodents in North America: the Geomyidae (pocket gophers) and the Heteromyidae (kangaroo rats, pocket mice, and their relatives). We assessed variation in skull morphology (including both shape and size) among geomyoids to test the hypothesis that there are statistically significant differences in skull measurements at the family, genus, and species levels. Our sample includes 886 specimens representing all geomyoid genera and 39 species. We used the geometric mean to compare size across taxa. We used 14 measurements of the cranium and lower jaw normalized for size to compare shape among and within taxa. Our results show that skull measurements enable the distinction of geomyoids at the family, genus, and species levels. There is a larger amount of size variation within Geomyidae than within Heteromyidae. Our phylomorphospace analysis shows that the skull shape of the common ancestor of all geomyoids was more similar to the common ancestor of heteromyids than that of geomyids. Geomyid skulls display negative allometry whereas heteromyid skulls display positive allometry. Within heteromyids, dipodomyines, and non-dipodomyines show significantly different allometric patterns. Future analyses including fossils will be necessary to test our evolutionary hypotheses.

Key words: canalization, convergent evolution, Geomyidae, Heteromyidae, morphometrics, phylomorphospace.

The superfamily Geomyoidea is one of the most species-rich rodent clades. It includes 109 species in 2 families: the Heteromyidae (kangaroo rats, pocket mice, and their relatives) and the Geomyidae (pocket gophers; Fabre et al. 2012; D'Elía et al. 2019; Upham et al. 2019; Mammal Diversity Database 2021). Geomyoids display large amounts of ecological variation. They are found across many different habitats (e.g. Anderson and Gutiérrez 2009; Braun et al. 2021; Cervantes 2021; Parsons et al. 2022). Their locomotion ranges from fossorial to semi-fossorial, terrestrial, and ricochetal (Bartholomew and Caswell 1951; Bartholomew and Cary 1954; Djawdan 1993; Wilkins and Roberts 2007; Calede et al. 2019) and their diets consist of roots and tubers, sometimes plant stems, incorporating grasses, fruits, and seeds (e.g. Martínez-Gallardo and Sánchez-Cordero 1993; Taylor et al. 2009; Connior 2011). The great taxonomic and ecological diversities of geomyoids are associated with an incredible disparity of skull morphologies (Hafner and Hafner 1988). Prior studies have explored the link between skull morphology and diet or locomotion in rodents including geomyoids (e.g. Samuels 2009; Verde Arregoitia et al. 2017; Calede et al. 2019; Scarpitti and Calede 2022). The link between skull morphology and taxonomy in geomyoids remains to be rigorously investigated, yet it may be important to identify taxa; both extant and fossil geomyoids can be difficult to identify in some contexts (Calede and Glusman 2017; Wyatt et al. 2021; Kays et al. 2022).

The systematics of Geomyoidea have been the subject of much attention (e.g. Demastes et al. 2002; Alexander and Riddle 2005; Belfiore et al. 2008; Hafner et al. 2008, 2009; Mathis et al. 2014; Riddle et al. 2014; Spradling et al. 2016). The family Heteromyidae is divided into the subfamilies Heteromyinae, composed of *Heteromys*; Dipodomyinae, composed of *Dipodomys* and *Microdipodops*; and Perognathinae, composed of *Chaetodipus* and *Perognathus*. All living Geomyidae are included in the subfamily Geomyinae (Anderson et al. 2006; Hafner et al. 2007; Fabre et al. 2012). Yet, despite the extensive amount of work dedicated to the systematics of Geomyoidea, phylogenetic uncertainty remains and the monophyly of Heteromyidae exclusive of Geomyidae is still debated (Alexander and Riddle 2005; Hafner et al. 2007; Fabre et al. 2012). Generally speaking, the taxonomy of Geomyoidea is an active area of research (e.g. ; Hafner et al. 2014; Mathis et al. 2014; Riddle et al. 2014; Spradling et al. 2016; Calede and Rasmussen 2020, Ortiz-Caballero et al. 2020; Gutiérrez-Costa et al. 2021) and morphology is a critical tool in the identification of geomyoid species and their relationships (e.g. Russell 1968; Baker and Williams 1974; Carrasco 2000; Hafner et al. 2004; Jones and Baxter 2004; Alexander and Riddle 2005; Hafner et al. 2005; Anderson and Gutierrez 2009; Hafner et al. 2011, 2014; Mathis et al. 2014; Calede and Glusman 2017; Wyatt et al. 2021). Skull morphology specifically has already been demonstrated to be

Received 12 March 2022; accepted 12 July 2022

informative in select geomyoids. Thus, the study of the skulls of *Heteromys* has enabled the recognition of new species and taxonomic revisions (Anderson and Jarrín-V 2002; Anderson 2003; Anderson and Timm 2006). Spradling et al. (2016) used skull morphology to clarify the taxonomy of *Heterogeomys* and *Orthogeomys*. Riddle et al. (2014) used morphometrics to explore cryptic diversity within a species of *Perognathus*.

Our goal is to determine the potential of morphology to inform taxonomy, quantify morphological disparity, and determine morphospace overlap across a broad sample of geomyoid species. We build upon Calede and Brown (2021), which quantified sexual dimorphism in skull shape and size in geomyoids and explore morphological variation in skull shape and size across taxa. Combined with phylogenetics, our morphological data enable an initial study of the pattern of skull shape evolution within Geomyoidea. It, therefore, leads us to quantify patterns previously recognized based on qualitative observations that Heteromyidae displays large disparity in skull morphology, whereas Geomyidae taxa show little shape variation and, instead, exemplify morphological convergence (Hafner and Hafner 1988). Our study is also an opportunity to compare the powers of tooth morphology (studied by Calede and Glusman [2017], Wyatt et al. [2021], and Carrasco [2000]) and skull morphology in deciphering geomyoid taxonomy. We test the following hypotheses: 1) size is an informative characteristic for geomyoid taxonomy; 2) skull shape helps distinguish Heteromyidae and Geomyidae at the family, genus, and species levels; 3) species within Geomyidae display high levels of convergence in skull shape; 4) Heteromyidae has higher morphological disparity than Geomyidae; 5) changes in allometric relationships between skull size and shape help explain the evolution of peculiar skull morphologies within Heteromyidae, particularly in Dipodomyinae.

Materials and Methods

Taxonomic sampling and data collection

Our sample is built upon that of Calede and Brown (2021), which analyzed sexual dimorphism in skull size and shape in geomyoids. It contains 886 specimens (Table 1). We included data from 396 geomyid specimens representing all 7 genera and 17 of 41 species as well as 490 heteromyid specimens representing all 5 genera and 22 of 68 species (mean 22.7 per species, median 18). Based on prior results of the sampling necessary to accurately quantify size and shape in geomyoids (Calede and Brown 2021), we included a minimum of 16 specimens per species in our analyses in all but one species. We only analyzed data from adult specimens (based on the fusion of cranial sutures and the presence of fully erupted worn teeth) to avoid ontogenetic effects on morphology. We included both males and females for every taxon, sampling a subequal or equal number of specimens for both sexes whenever possible. Whenever possible, we sampled specimens across a large proportion of the geographic range for the species to cover geographic and environmental variation. The role of geographic variation in geomyoid morphology is discussed in part in Calede and Brown (2021). We also included, when possible, a range of sampling expedition dates, in part by selecting specimens across museums. Only 1 species (*Cratogeomys merriami*) was sampled from a single museum, yet our sample for this species still spans 5 different provinces of Mexico and 3 different collection years.

For each specimen, we measured 14 skull variables representing skull shape in 3 dimensions (length, width, and depth) across 4 regions of the skull (rostrum, palate, braincase, and lower jaw; Figure 1, Table 2). Measurements were taken from a prior analysis of morphological variation in geomyoids (Calede and Brown 2021), photos of the specimens using ImageJ 1.51 (Schneider et al. 2012), or directly from specimens using "Mitutoyo CD-6" CSX digital calipers. Photos were taken using a Canon EOS Rebel SL2 camera and a copy stand or gathered from public online museum repositories. Measurements not on the mid-sagittal plane were taken on the left side of the specimen when possible; the right when the left side was not available. All measurements were logged prior to analyses except for the calculations of the multivariate coefficient of variation (see below) for which negative log values would skew the results. For each specimen, we calculated the geometric mean of the measurements using the square root of the product of all 14 measurements (Jungers et al. 1995, Madar et al. 2002). We normalized the data for size by dividing each measurement by the geometric mean resulting in a new variable that represents form and can be compared across specimens of different sizes (Calede and Brown 2021). The complete dataset is provided in Supplementary Data 1. The phylogenetic framework we used is from Fabre et al. (2012). We randomly selected 100 trees from the 1000 time-calibrated trees developed by Price and Hopkins (2015) and pruned the trees to keep taxa with morphological data using the package ape 5.5 (Paradis et al. 2004) in R 4.0.5 (R Core Team 2019).

Measurement errors

Measurements were recorded to the nearest 0.01 mm. Data checks were performed across the entire dataset by the senior author to assess the reliability of measurements. These checks included remeasuring specimens measured once using ImageJ or calipers using the same technique and remeasuring specimens measured with calipers using photos (in ImageJ). A subset of specimens was selected at random from the entire dataset to assess possible errors in the measurements made from photographs. This sample covered all species included in this study measured using photographs. For the 2 comparisons involving calipers, a smaller number of specimens selected randomly across species covering both heteromyids and geomyids was selected. The absolute difference in millimeters between the first and second measurements was computed. Errors reported as percentages were calculated relative to the initial measurement. The effects on the analyses were assessed by rerunning the analyses (including geometric mean calculations and skull shape analyses). These measurement errors were assessed and reported on by Calede and Brown (2021).

Analyses of size and shape

We used Shapiro–Wilk tests to test for normality in the distribution of our size data. Based on the results, we used Kruskal–Wallis tests to assess statistical differences in geometric means among the 17 geomyid species and 22 heteromyid species studied. The significant tests were followed by post hoc Tukey honest significance tests (THSD) to investigate pairwise differences. We predicted that skull size is significantly different among genera within each family, and across species within each genus based on prior analyses of size in geomyoids (e.g. Calede and Brown 2021; Wyatt et al. 2021).

Table 1. Sample of geomyoid rodents included in this study

Family	Subfamily	Genus	Species	F	M	Abbreviations
Geomyidae	Geomyinae	*Cratogeomys*	*castanops*	10	14	Ccs
Geomyidae	Geomyinae	*Cratogeomys*	*fumosus*	9	10	Cfu
Geomyidae	Geomyinae	*Cratogeomys*	*merriami*	12	12	Cme
Geomyidae	Geomyinae	*Geomys*	*arenarius*	9	9	Gar
Geomyidae	Geomyinae	*Geomys*	*bursarius*	8	10	Gbu
Geomyidae	Geomyinae	*Geomys*	*personatus*	8	8	Gpe
Geomyidae	Geomyinae	*Geomys*	*pinetis*	15	12	Gpi
Geomyidae	Geomyinae	*Heterogeomys*	*heterodus*	9	9	Hhe
Geomyidae	Geomyinae	*Heterogeomys*	*hispidus*	9	8	Hhi
Geomyidae	Geomyinae	*Orthogeomys*	*grandis*	14	15	Ogr
Geomyidae	Geomyinae	*Pappogeomys*	*bulleri*	12	13	Pbu
Geomyidae	Geomyinae	*Thomomys*	*bottae*	26	23	Tbo
Geomyidae	Geomyinae	*Thomomys*	*monticola*	6	9	Tmo
Geomyidae	Geomyinae	*Thomomys*	*talpoides*	15	15	Tta
Geomyidae	Geomyinae	*Thomomys*	*townsendii*	12	11	Tto
Geomyidae	Geomyinae	*Thomomys*	*umbrinus*	12	12	Tum
Geomyidae	Geomyinae	*Zygogeomys*	*trichopus*	10	10	Ztr
Heteromyidae	Dipodomyinae	*Dipodomys*	*deserti*	9	10	Dde
Heteromyidae	Dipodomyinae	*Dipodomys*	*heermanni*	10	13	Dhe
Heteromyidae	Dipodomyinae	*Dipodomys*	*ingens*	9	9	Din
Heteromyidae	Dipodomyinae	*Dipodomys*	*merriami*	24	25	Dme
Heteromyidae	Dipodomyinae	*Dipodomys*	*ordii*	20	20	Dor
Heteromyidae	Dipodomyinae	*Dipodomys*	*spectabilis*	9	9	Dsp
Heteromyidae	Dipodomyinae	*Microdipodops*	*megacephalus*	10	14	Mme
Heteromyidae	Dipodomyinae	*Microdipodops*	*pallidus*	10	11	Mpa
Heteromyidae	Heteromyinae	*Heteromys*	*anomalus*	8	8	Han
Heteromyidae	Heteromyinae	*Heteromys*	*desmarestianus*	9	8	Hde
Heteromyidae	Heteromyinae	*Heteromys*	*gaumeri*	8	8	Hga
Heteromyidae	Heteromyinae	*Heteromys*	*irroratus*	11	10	Hir
Heteromyidae	Heteromyinae	*Heteromys*	*pictus*	9	10	Hpi
Heteromyidae	Perognathinae	*Chaetodipus*	*baileyi*	9	9	Cba
Heteromyidae	Perognathinae	*Chaetodipus*	*californicus*	9	12	Ccl
Heteromyidae	Perognathinae	*Chaetodipus*	*hispidus*	8	8	Chi
Heteromyidae	Perognathinae	*Chaetodipus*	*intermedius*	15	17	Cin
Heteromyidae	Perognathinae	*Chaetodipus*	*penicillatus*	11	11	Cpe
Heteromyidae	Perognathinae	*Perognathus*	*flavescens*	8	8	Pfl
Heteromyidae	Perognathinae	*Perognathus*	*flavus*	8	9	Pfu
Heteromyidae	Perognathinae	*Perognathus*	*longimembris*	11	12	Plo
Heteromyidae	Perognathinae	*Perognathus*	*parvus*	11	13	Ppa

Abbreviations: F, number of female specimens; M, number of male specimens.

The 14 skull measurements were included in a principal component analysis (PCA) to explore morphospace occupation at the superfamily level (Geomyoidea). The PCA was repeated at lower taxonomic levels to assess similarities and differences in skull morphology among genera and species. Eigenvalues were determined for each of the principal components identified and eigenvectors were used to assess the weight of skull features on the overall eigenvalue. We only retained significant axes in our analyses. The determination was made using a Monte Carlo randomization test run in biostats (McGarigal 2015). PCAs were followed by a multivariate analysis of variance (MANOVA), to assess statistical differences. Significant MANOVAs were followed by ANOVAs and THSDs on individual principal components as appropriate to interpret the pattern of morphological variation. We predicted that there would be statistically significant differences in skull measurements among taxa.

We used a phylomorphospace to overlay phylogenetic information on the mean PC scores for each species using phytools 0.7-80 (Sidlauskas 2008, Revell 2012). This enabled us to explore the pattern of evolution of skull morphology within Geomyoidea and test the hypotheses of Hafner and Hafner (1988) that geomyids are highly convergent in

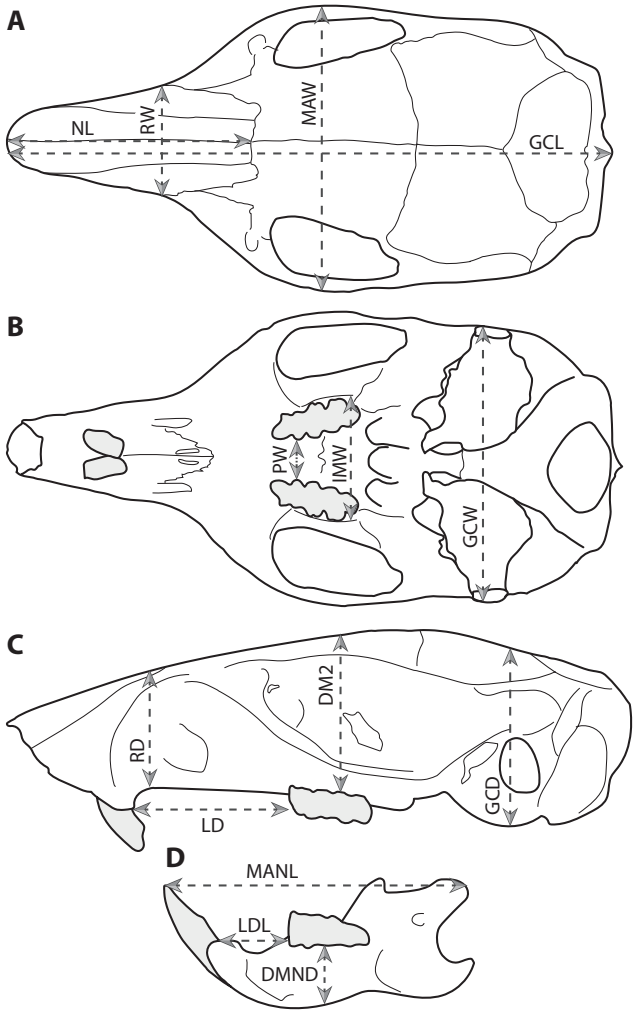

Figure 1. Cranial measurements used in the analyses. (A) Cranium in dorsal view. (B) Cranium in ventral view. (C) Cranium in lateral view. (D) Dentary in medial view. Abbreviations defined in Table 2. Figure from Calede and Brown (2021).

skull shape whereas heteromyids display a large disparity in skull shape.

The transformed skull variables were used in a series of canonical variate analyses (CVA) run at the family, genus, and species levels to determine the usefulness of skull morphology in classifying specimens into their taxonomic groups. We used a jackknife to assess how reliably each taxon in the training set can be assigned to their a priori taxonomic category (Strauss 2010). We predicted that skull measurements help identify specimens at all taxonomic levels based on qualitative observations of skulls and published case studies (Anderson and Jarrín-V 2002; Anderson 2003; Anderson and Timm 2006; Riddle et al. 2014; Spradling et al. 2016).

Morphological variation

Prior analyses of variation in geomyoids have focused on intraspecific variation in isolated taxa using univariate statistics (e.g. Desha 1967). Here, we used all 14 variables in our analyses to calculate the multivariate coefficient of variation (multiCV) for each family, genus, and species. We followed the approach of Lal et al. (2015) originally described by Van Valen (1978) and used by Soulé and Zegers (1996) in a prior analysis of the geomyid taxon *Thomomys bottae*. We predicted higher multiCV values for Heteromyidae than Geomyidae and greater variation in multiCV across Heteromyidae genera based on qualitative observations of skulls and prior research (Hafner and Hafner 1988). We explored the relationship between size and multiCV using a phylogenetic generalized least squares regression (PGLS). We expected a statistically significant regression with increased variation associated with increased size, as a consequence of the uniquely enlarged bullae found in Dipodomyinae.

Allometry

We used PGLS in caper 1.0.1 (Orme 2018) to analyze allometry at the family level and determine the possible covariance

Table 2. Description of the measurements used in the analyses

Abbreviations	Description
GCL	Greatest cranium length from anterior edge of nasal to posterior edge of skull
NL	Nasal length
IMW	Intermaxillary width at M3
MAW	Maxillary arch width at widest point
GCD	Greatest cranium depth from dorsal edge of parietal to ventral edge of auditory bulla
GCW	Greatest cranium width across tympanic bullae
RW	Rostral width
RD	Rostral depth
DM2	Depth of skull at M2 alveolus
PW	Palatine width between toothrows at P4
LD	Length of upper diastema
LDL	Length of lower diastema
DMND	Depth of dentary at m1
MANL	Mandibular length from anterior face of incisor to posterior edge of condyloid process

Note: Abbreviation used in Figures 2–8.

of size and shape. Allometric analyses were run separately for the 2 families. The natural log of the geometric mean was used as the *x*-axis variable; PC values were used for the y-axis. The PGLS was run on all 100 trees to account for uncertainties in branch lengths. For the Heteromyidae, we ran follow-up PGLS analyses for the Dipodomyinae and non-dipodomyine heteromyids to further explore the role of allometry in the peculiar inflated bullae of dipodomyines. When discussing the allometric scaling of individual morphological variables, we only retained those with the highest eigenvectors.

Results

Measurement errors

As previously reported in Calede and Brown (2021) for a subset of the dataset studied herein, errors in our measurements are minimal; they range from <0.2% to under 9%. There is no evidence that 1 of the 2 methods (measurements using calipers or from photographs) leads to higher errors. Errors are largest (as a %) for the smallest variables measured (PW and DMND), which were sometimes <1.5 mm. There is no other systematic pattern of bias. The largest error only affected the geometric mean value by 1%. A theoretical application of the worst measurement error detected to all 14 measurements of the smallest specimen in the dataset yields a change in the log of the geometric mean for that specimen of only 4.6%. We could not detect any effect on our multivariate analyses of the shape of measurement errors.

Size

There is a dispersion of geomyid species' geometric means between 7.9 and 20.1. The means range between 5.3 and 12.6 in Heteromyidae (Figure 2). There is a greater size variation in geomyid species than heteromyid species. The size distribution in each of the 2 families is not normally distributed (Geomyidae: $W = 0.974$, $P < 0.001$; Heteromyidae: $W = 0.966$, $P < 0.001$). Within Geomyidae, *Geomys* and *Thomomys* have the largest range of values. Within heteromyids, *Perognathus longimembris*, *Heteromys gaumeri*, *and Chaetodipus hispidus* have the largest range of values. Skull size is significantly different among species within both geomyids (Kruskal–Wallis: $\chi^2 = 347.65$, $P < 0.001$, $R^2 = 0.88$) and heteromyids (Kruskal–Wallis: $\chi^2 = 467.93$, $P < 0.001$, $R^2 = 0.96$); it is also significantly different among genera in both families (Kruskal–Wallis: $\chi^2 = 303.52$, $P < 0.001$, $R^2 = 0.77$ and $\chi^2 = 419.02$, $P < 0.001$, $R^2 = 0.85$, respectively). Among geomyids, only 3 pairs of genera are not significantly different in size: *Orthogeomys* and *Heterogeomys*, *Zygogeomys* and *Cratogeomys*, as well as *Thomomys* and *Pappogeomys*. Within Heteromyidae, only *Microdipodops* and *Chaetodipus* are not significantly different in size. Post hoc comparisons show significant differences in over 82% of the species pairs within Geomyidae; only 8 pairs that are not significantly different are congeneric (Supplementary Data 2), and 90% of taxon pairs within Heteromyidae, only 7 that are not significantly different are congeneric (Supplementary Data 3).

Phylomorphospace and family-level differences

The 2 families occupy distinct regions of the morphospace (MANOVA: $F = 4788.8$, $P < 0.001$; Figure 3) and differ significantly along PC1 (ANOVA: $F = 760.9$, $P < 0.001$, $R^2 = 0.97$). All geomyids have negative PC1 scores, which correspond to broader zygomatic arches (MAW), larger mandible length (MANL), longer diastemata (LD, LDL), deeper mandibles (DMND), and deeper maxillary regions (DM2) (Supplementary Data 4). Heteromyids have positive PC1 scores, which correspond to wider palates (PW) and longer skulls (GCL). There is a greater disparity among Heteromyidae than Geomyidae along PC2; heteromyids span all of PC2. *Heteromys* displays the lowest PC2 scores (larger rostral width [RW] and narrower skulls [low MAW and GCW]). Dipodomyines occupy the positive end of PC2 (broader and deeper skulls but very narrow rostra). Perognathines occupy an intermediate position ($-1 <$ PC2 scores < 1). The most recent common ancestor of Heteromyidae is reconstructed to be most similar in morphology to *Chaetodipus*. The most recent common ancestor of Geomyoidea is itself reconstructed as very similar to the common ancestor of Heteromyidae. The most recent common ancestor of Geomyidae is estimated to be most similar in morphology to *Thomomys*. The CVA shows that both families are 100% correctly identified a posteriori (Figure 4A).

Genus-level variation

The PCA of the Geomyidae shows distinct morphospace occupation across genera (MANOVA: $F = 21.85$, $P < 0.001$). The 2 significant axes explain over 34% of the variance (Figure 5A). PC1 is positively correlated with IMW, GCD, and DMND and negatively correlated with LD, LDL, and MRD. PC2 is positively correlated with GCW and RW and negatively correlated with PW (Supplementary Data 4). *Orthogeomys* and *Geomys* have negative PC1 scores. *Pappogeomys* has positive PC1 scores. *Heterogeomys*, *Zygogeomys*, and *Cratogeomys* occupy intermediate values; *Thomomys* range across most of PC1. *Thomomys* and *Geomys* cluster at the negative end of PC2; *Zygogeomys*, *Heterogeomys*, and *Cratogeomys* cluster at the positive end. The PCA of the Heteromyidae also shows distinct morphospace occupation across genera (MANOVA: $F = 184.4$, $P < 0.001$). The 2 significant axes explain over 53% of the variance (Figure 5B). PC1 is positively correlated with MANL, RW, LD, and NL, and negatively correlated with GCW, GCD, and PW. PC2 is positively correlated with GCL and IMW, and negatively correlated with MAW, LDL, and DMND. *Microdipodops* has the most negative PC1 scores; *Heteromys* and *Chaetodipus* have positive PC1 scores. *Dipodomys* and *Perognathus* occupy intermediate values.

The first axis of the genus-level CVA for the Geomyidae (Figure 4B) represents 60.9% of the variance; CV2 17.6%. Positive CV1 scores correspond to larger GCL, MAW, and GCD; negative CV1 scores correspond to larger RW, GCW, and DM2. Positive CV2 scores represent larger MANL and DM2; negative CV2 scores represent larger LDL, GCW, GCD, and MAW. *Cratogeomys* has positive PC1 and PC2 values. *Heterogeomys* and *Orthogeomys* have negative PC1 values, but positive PC2 values. *Thomomys* has negative PC1 and PC2 values; *Pappogeomys*, *Zygogeomys*, and *Geomys* have positive PC1, but negative PC2 values. In the heteromyid analysis (Figure 4C), CV1 represents 74.5% of the variation; CV2 17.3%. Positive CV1 scores are associated with larger GCW and MAW. Negative CV1 scores correspond to larger MANL. Positive CV2 scores correspond to larger GCL whereas negative CV2 scores correspond to larger MAW. *Heteromys* is characterized by negative CV1 scores and CV2 scores around zero; *Perognathus* and *Chaetodipus* also have CV2 scores

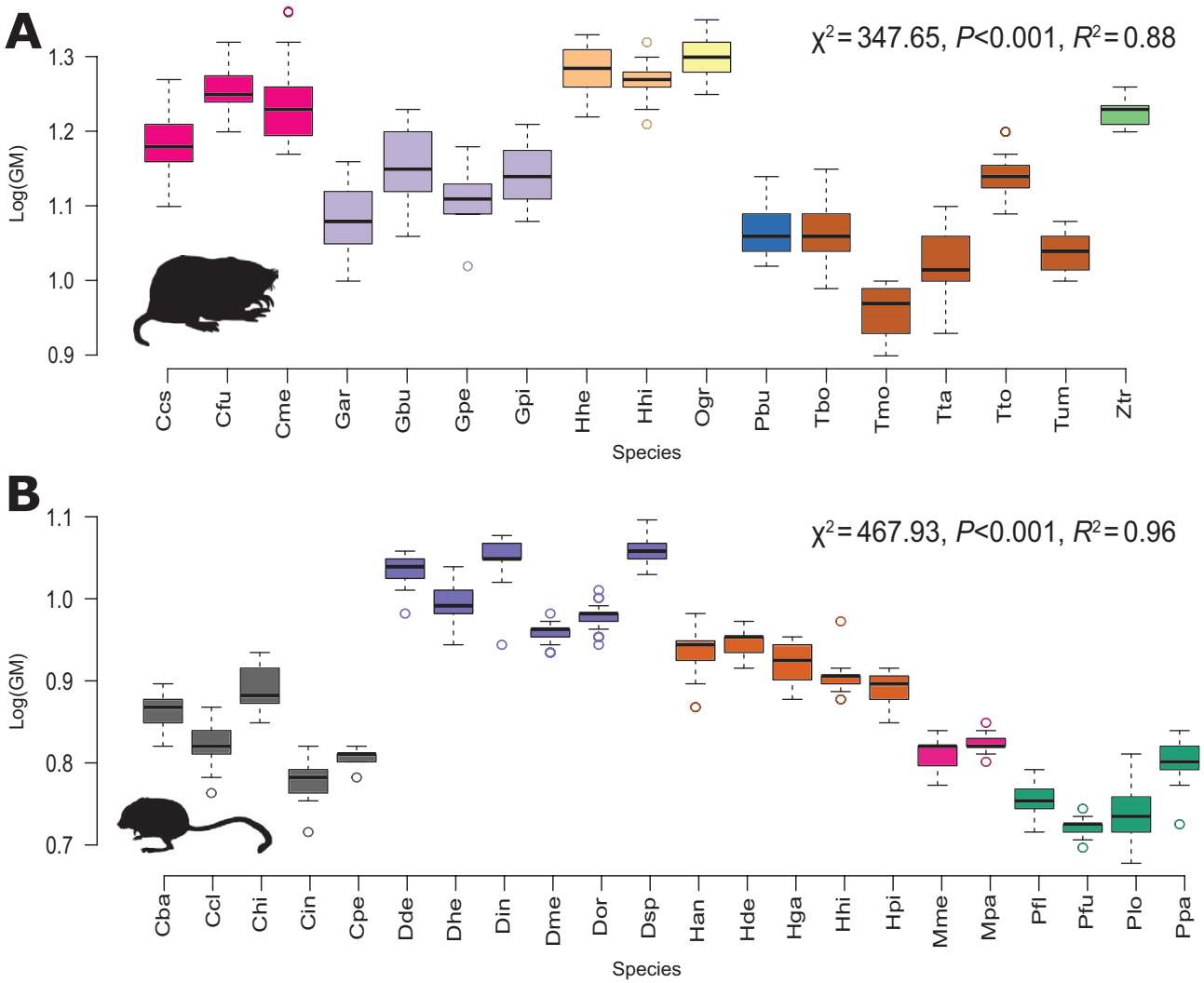

Figure 2. Results of the size comparison among species of geomyoids. (A) Size variation within Geomyidae. (B) Size variation within Heteromyidae. Abbreviations for species names are provided in Table 1.

distributed around zero, but more positive CV1 values than *Heteromys*. *Microdipodops* has both positive CV1 and positive CV2 scores. *Dipodomys* has positive CV1 scores and negative CV2 scores. Within Geomyidae, specimens of *Zygogeomys* are correctly identified most accurately (90%). *Thomomys* specimens are accurately identified at a slightly lower rate of 84.4%. *Cratogeomys* and *Heterogeomys* have accurate classification rates around 75%. *Orthogeomys* and *Geomys* have accurate classification rates above 60%. *Pappogeomys* has the lowest accurate rate of classification (40%). Within Heteromyidae, all genera are accurately identified at rates at or above 80%. Both *Microdipodops* and *Dipodomys* are correctly identified 100% of the time. *Heteromys* is accurately identified 92% of the time. *Chaetodipus* and *Perognathus* have the lowest accurate classification rates for the family at 81.2 and 80%, respectively.

Species-level variation

Cratogeomys

The PCA of *Cratogeomys* (Figure 6A) shows significant differences among species (MANOVA: $F = 24.9$, $P < 0.001$). PC1 accounts for 21.5% of the variance in the dataset; PC2 14.5%. The PC1 scores of the 3 species are significantly different (ANOVA: $F = 24.5$, $P < 0.001$, $R^2 = 0.43$). PC1 is positively correlated with MAW and negatively correlated with DM2, MRD, GCD, and PW (Supplementary Data 4). *Cratogeomys fumosus* occupies the positive end of PC1. A post hoc Tukey test demonstrates that *C. fumosus* is significantly different from the other 2 species in PC1 scores (both THSD $P < 0.001$). PC2 is positively correlated with NL and negatively correlated with PW and IMW. The 3 species are significantly different (ANOVA: $F = 9.75$, $P < 0.001$, $R^2 = 0.23$). *Cratogeomys merriami* has higher PC2 scores than the other 2 species (THSD: $P < 0.001$ for both comparisons).

CV1 explains 72.9% of the variation; CV2 27.1% (Figure 8A). Positive CV1 scores correspond to larger GCW and IMW; negative CV1 scores correspond to larger DM2 and LDL. Positive CV2 scores correspond to a larger DM2; negative CV2 scores correspond to a larger LDL. *Cratogeomys castanops* has low CV1 and CV2 scores; *C. fumosus* has low CV2 but high CV1 scores; specimens of *C. merriami* have high CV1 scores and intermediate CV2 scores. *Cratogeomys castanops* was identified correctly 92% of the time, *C. fumosus* 84% of the time, and *C. merriami* 79% of the time.

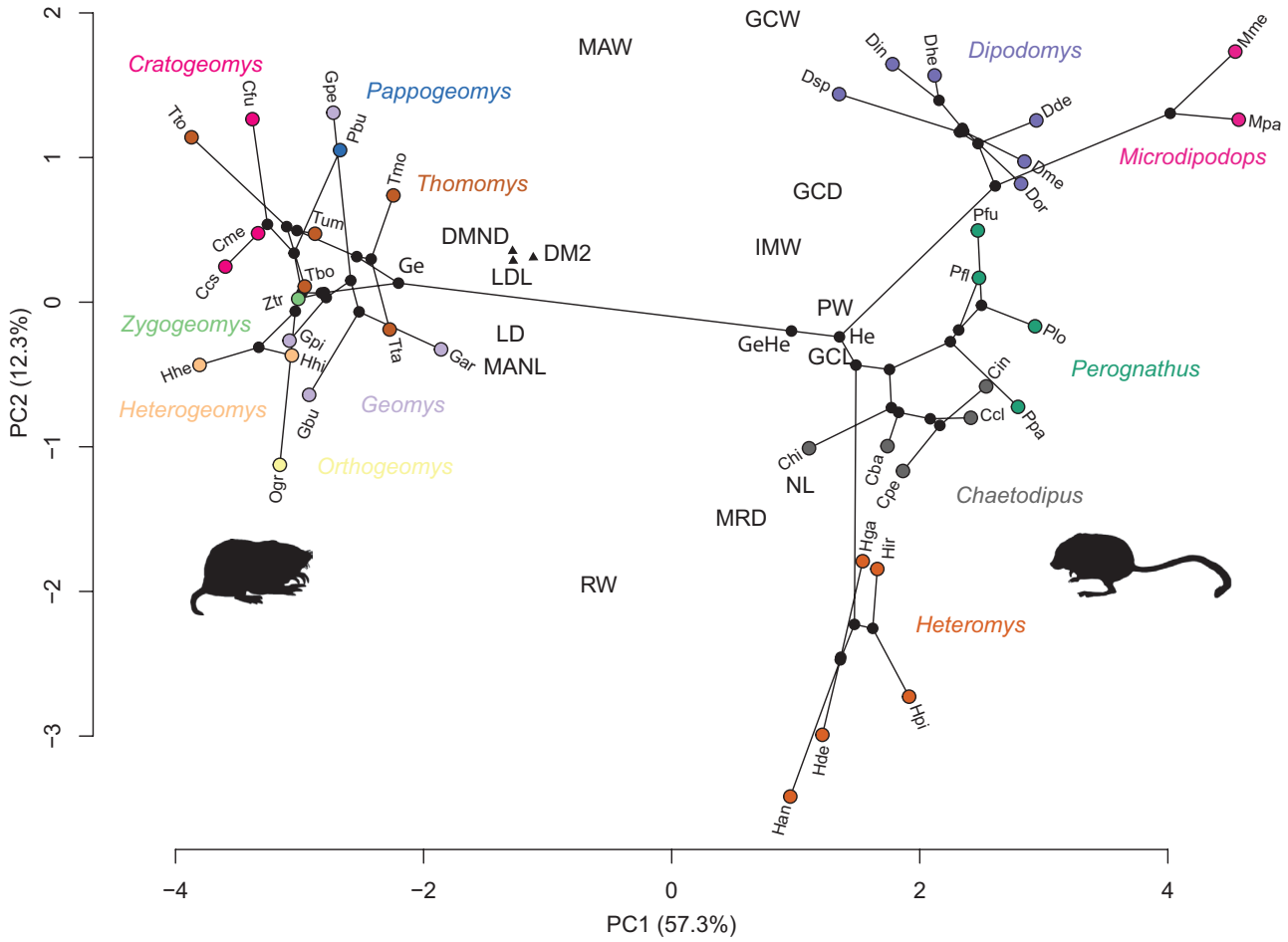

Figure 3. Phylomorphospace for the 39 Geomyoidea species studied. Geomyids are clustered to the left of the morphospace; heteromyids are located on the right of the morphospace. Each point represents a species. Black dots represent reconstructed ancestral character states. Genera are color coded. See Table 1 for species abbreviations and Table 2 for skull measurement abbreviations. Abbreviations: Ge, common ancestor of Geomyidae; GeHe, common ancestor of Geomyoidea; He, common ancestor of Heteromyidae.

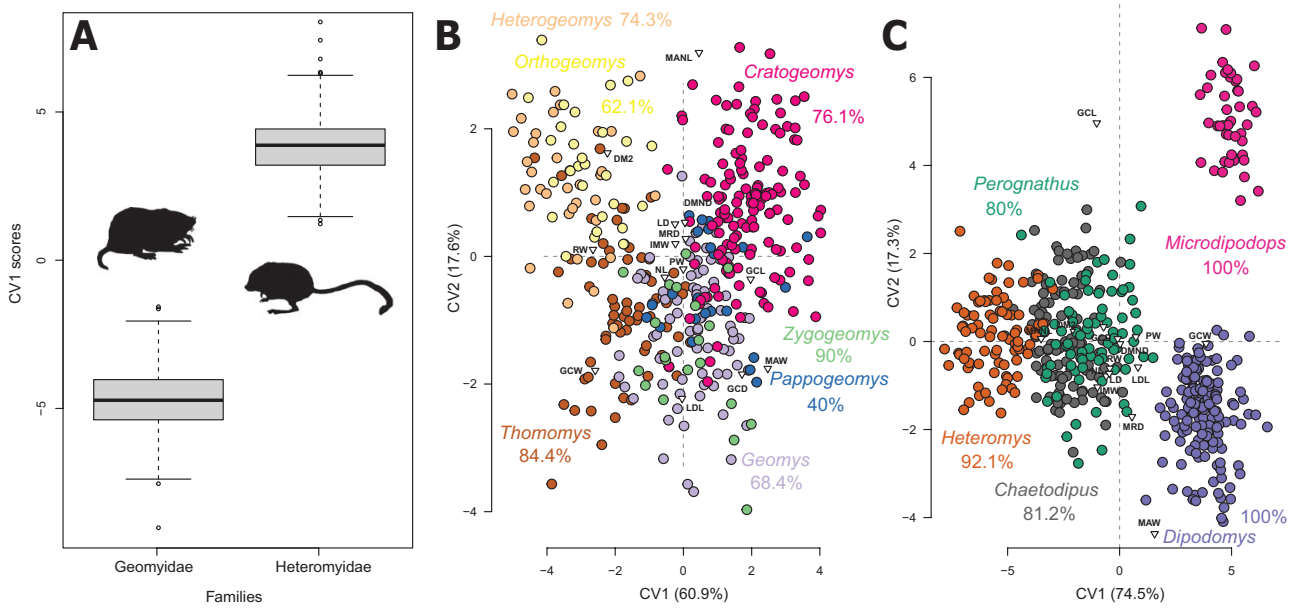

Figure 4. Canonical variate analyses at the family and genus levels. (A) Family-level analysis. (B) Genus-level within family Geomyidae. (C) Genus-level within family Heteromyidae. Each point represents a specimen. Genera are color coded. See Table 2 for skull measurement abbreviations.

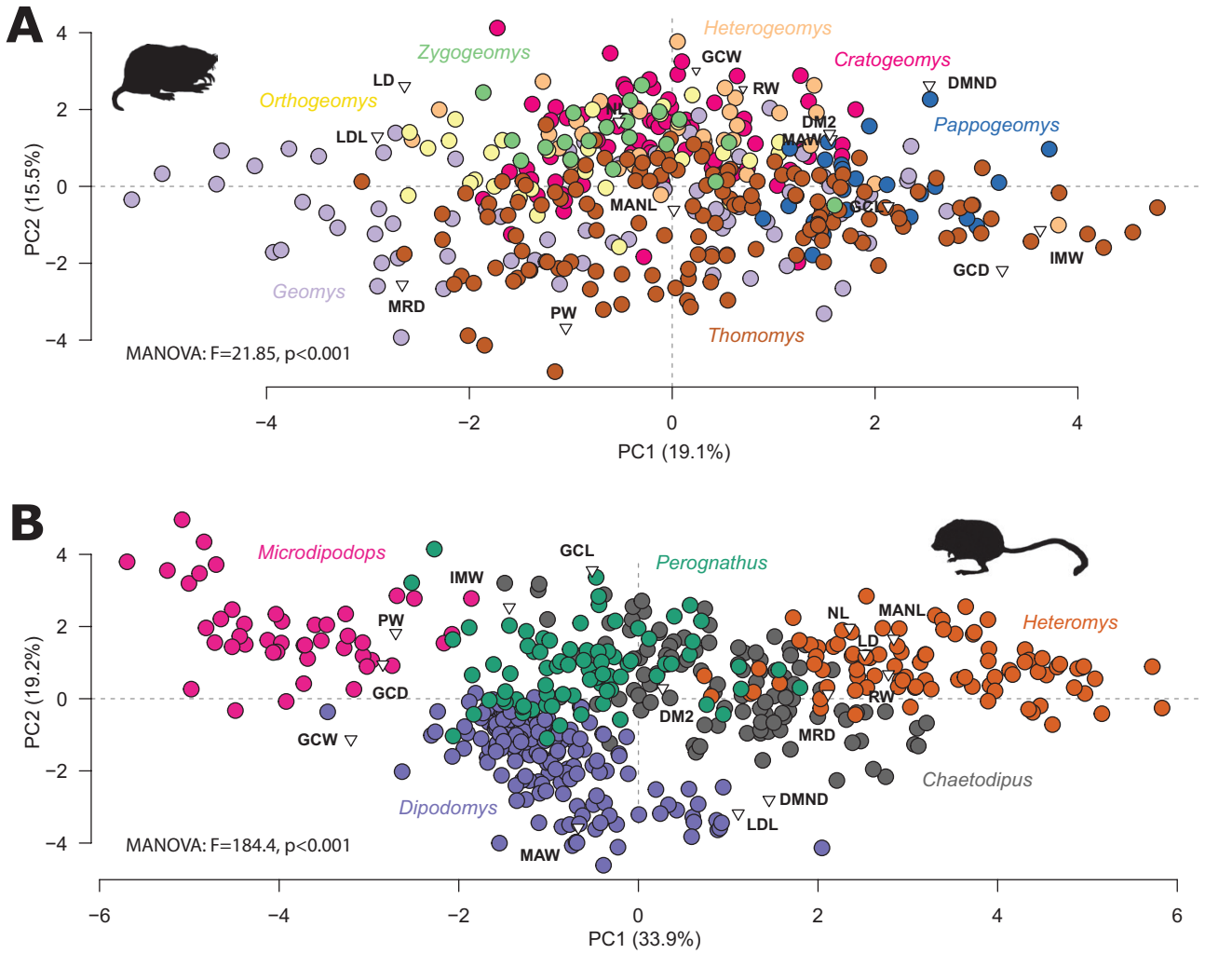

Figure 5. Principal component analyses showing shape variation within (A) Geomyidae and (B) Heteromyidae. Each point represents a specimen. Genera are color coded. See Table 2 for skull measurement abbreviations.

Geomys

Geomys species occupy distinct regions of the morphospace (Figure 6B; MANOVA: $F = 14.05$, $P < 0.001$). The 3 significant axes explain over 65% of the variance in the dataset. The PC1 scores of the 4 species are significantly different (ANOVA: $F = 25.29$, $P < 0.001$, $R^2 = 0.50$). PC1 is positively correlated with LDL and LD; negatively correlated with GCD, IMW, and DM2 (Supplementary Data 4). *Geomys pinetis* and *G. bursarius* occupy the positive end of PC1 whereas *G. personatus* and *G. arenarius* occupy the negative end of the axis. The species within each of these 2 clusters do not differ significantly from one another but species across clusters do (P values <0.001). PC2 is positively correlated with LD and negatively correlated with PW. The PC2 scores are significantly different across species (ANOVA: $F = 13.82$, $P < 0.001$, $R^2 = 0.36$). *Geomys personatus* displays positive PC2 scores whereas *G. arenarius* displays negative PC2 scores. All species differ significantly from one another in PC2 scores (P values <0.03), except *G. pinetis* and *G. bursarius*. CV1 accounts for 55.7% of the variation (Figure 8B). Positive CV1 scores correspond to larger GCL and LD; negative CV1 scores correspond to a larger MAW. CV2 accounts for 36.4% of the variation. Positive CV2 scores correspond to a larger MRD; negative CV2 scores correspond to larger MANL, GCW, and GCL. *Geomys bursarius*, *G. arenarius*, and *G. pinetis* have high PC2 scores; *G. personatus* specimens have low CV2 scores. *Geomys arenarius* was correctly identified over 83% of the time; the classification rate for *G. bursarius* is somewhat lower at 72%. Classification rates for *G. personatus* and *G. pinetis* are the highest (>92%).

Heterogeomys

The 2 species of *Heterogeomys* occupy distinct regions of the morphospace (Figure 6C; MANOVA: $F = 12.8$, $P < 0.001$). The first 2 axes of the PCA account for 42.2% of the variance in the dataset. The 2 species differ significantly in PC1 scores (t-test: $t = 4.8$, df = 32.7, $P < 0.001$). PC1 is positively correlated with LDL, LD, DM2, and MANL, and negatively correlated with MAW, PW, and GCW (Supplementary Data 4). *Heterogeomys hispidus* occupies the negative end of PC1, and *H. heterodus* the positive end. PC2 is positively correlated with IMW and GCD; negatively correlated with MRD and NL.

Heterogeomys heterodus occupies the negative end of CV1, *H. hispidus* the positive end (Figure 8C). *Heterogeomys heterodus* is classified correctly 88% of the time; *H. hispidus* 77.8%.

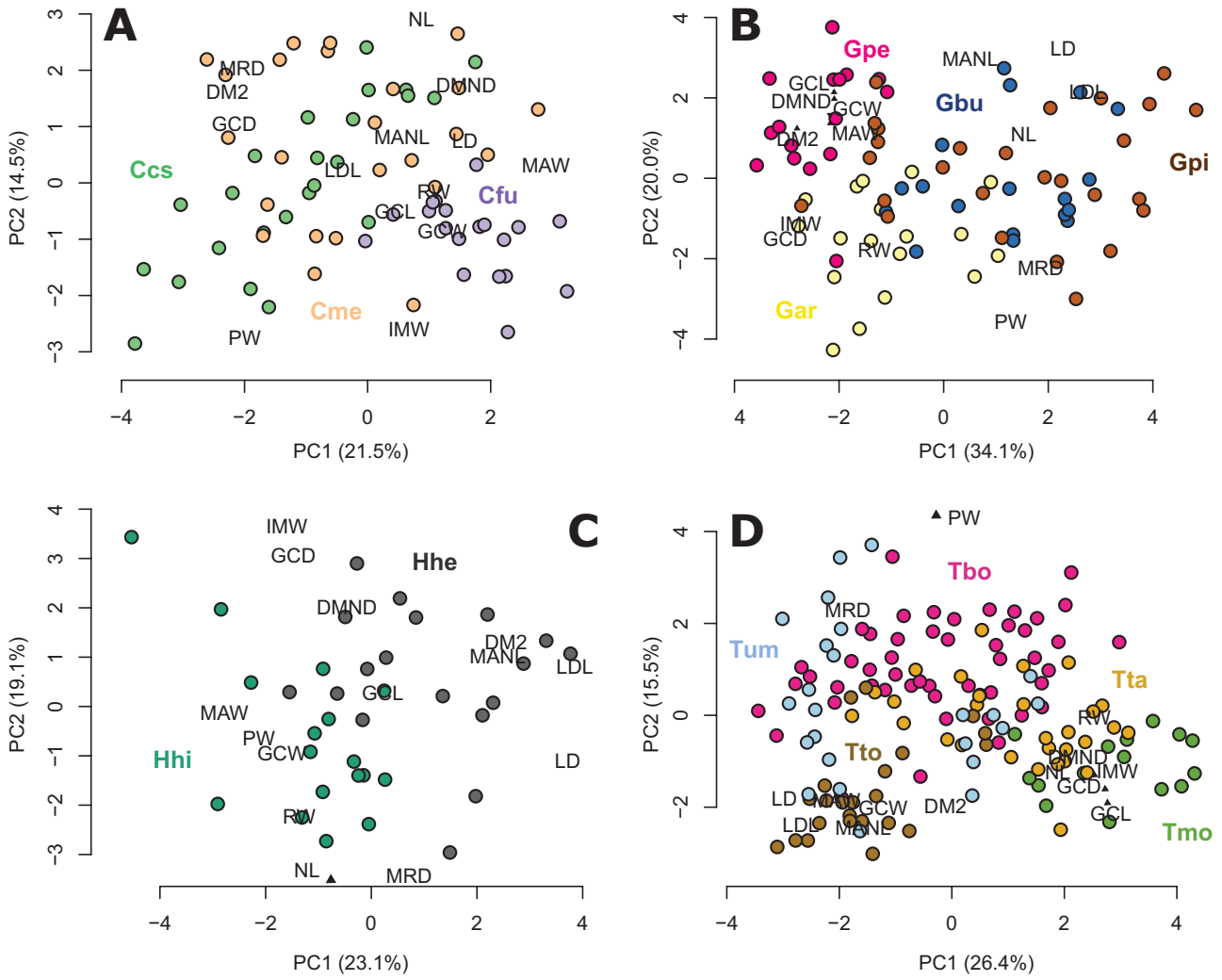

Figure 6. Principal component analyses showing variation within genera for Geomyidae: (A) *Cratogeomys*, (B) *Geomys*, (C) *Heterogeomys*, and (D) *Thomomys*. Species are color coded. See Table 1 for species abbreviations and Table 2 for skull measurement abbreviations.

Thomomys

The 5 species of *Thomomys* occupy distinct regions of the morphospace (Figure 6D; MANOVA: $F = 16.6$, $P < 0.001$). There are 4 significant axes explaining the variance in the dataset (PC1 represents 26.4%, PC2 15.5%). The PC1 scores of the 5 species are significantly different (ANOVA: $F = 34.28$, $P < 0.001$, $R^2 = 0.50$). PC1 is positively correlated with IMW, RW, GCL, and GCD and negatively correlated with LD and LDL (Supplementary Data 4). *Thomomys monticola* and *T. talpoides* occupy the positive end of PC1 whereas *T. townsendii* and most specimens of *T. umbrinus* occupy the negative end of the axis. The remaining specimens of *T. townsendii* have positive PC1 scores. All species of *Thomomys* differ significantly from one another except for the pair *T. umbrinus*–*T. townsendii* ($P = 0.97$). PC2 is positively correlated with PW and negatively correlated with several morphological variables including MANL, LDL, and GCW. The PC2 scores of the 5 species are significantly different (ANOVA: $F = 28.73$, $P < 0.001$, $R^2 = 0.46$). *Thomomys monticola*, *T. townsendii*, and *T. talpoides* occupy the negative end of PC2 whereas *T. bottae* occupies the positive end. *Thomomys umbrinus* ranges widely along PC2. All species pairs of *Thomomys* differ significantly except for *T. monticola*–*T. townsendii* ($P = 0.54$) and *T. umbrinus*–*T. talpoides* ($P = 0.59$).

CV1 accounts for 53.8% of the variation (Figure 8D). It is positively correlated with GCL and negatively correlated with MAW. *Thomomys monticola* and *T. talpoides* occupy the positive end of CV1; the other 3 species the negative end of the axis. CV2 accounts for 26.3% of the variation. Positive CV2 scores correspond to larger IMW and DM2 particularly; negative CV2 scores correspond to larger RW and GCL. *Thomomys townsendii* occupies the positive end of the axis whereas *T. bottae* occupies the negative end of PC2. The other species are intermediate. *Thomomys talpoides* was accurately classified 70% of the time, *T. townsendii* over 78% of the time, and *T. monticola* over 93% of the time; *T. umbrinus* and *T. bottae* were correctly identified 54% and 67% of the time, respectively.

Chaetodipus

The 5 species of *Chaetodipus* (Figure 7A) differ significantly in shape (MANOVA: $F = 8.8$, $P < 0.001$). The first 2 of the 4 significant axes account for nearly 39% of the variance. PC1 is positively correlated with DMND and LDL; it is negatively correlated with IMW, GCL, GCW, PW, and GCD (Supplementary Data 4). *Chaetodipus intermedius* and *C. californicus* occupy the negative end of PC1; the other 3 species the positive end (Figure 7A). The PC1 scores are significantly different among all species (ANOVA: $F = 29.8$, $P < 0.001$,

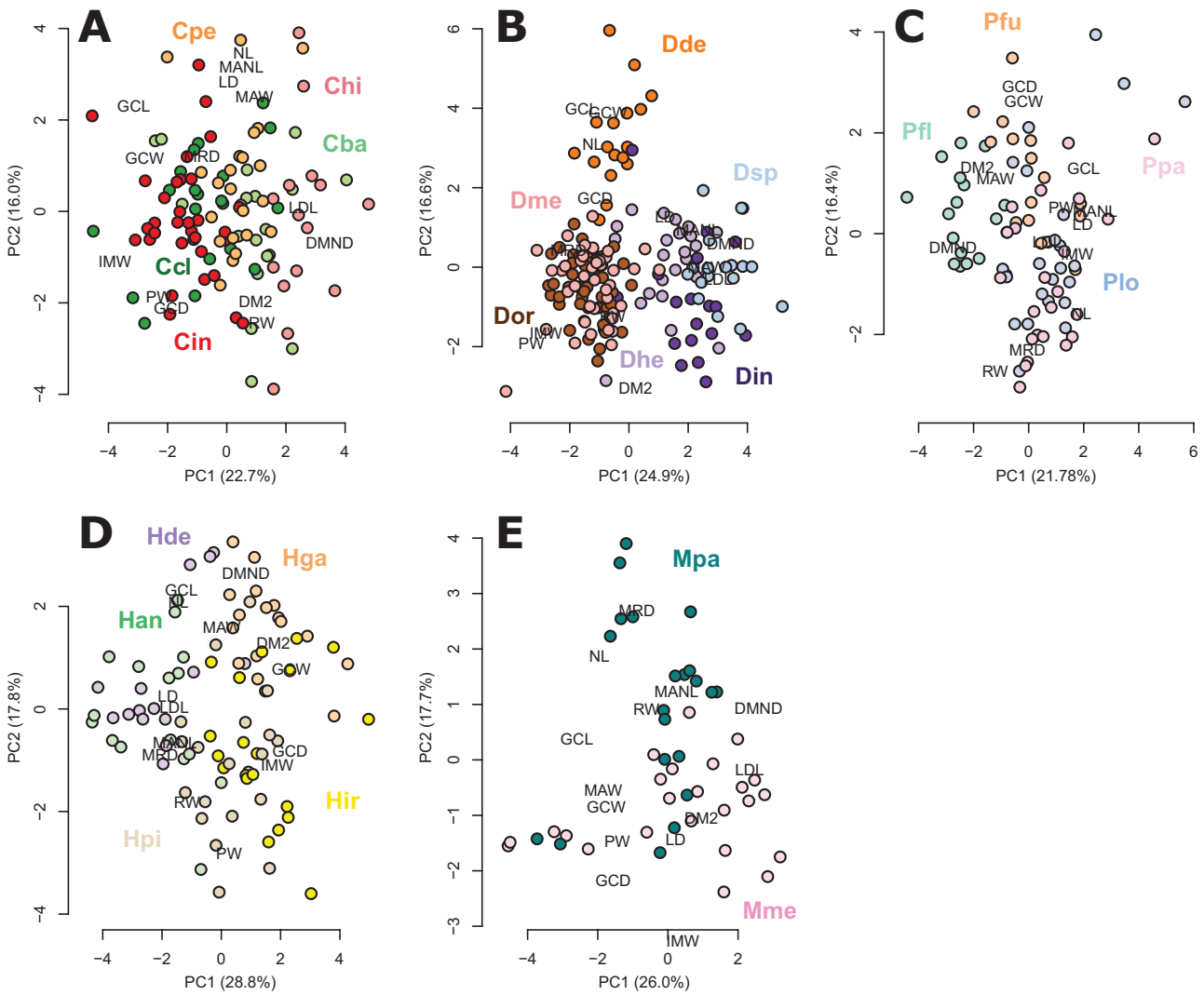

Figure 7. Principal component analyses showing variation within genera for Heteromyidae: (A) *Chaetodipus*, (B) *Dipodomys*, (C) *Perognathus*, (D) *Heteromys*, and (E) *Microdipodops*. Species are color coded. See Table 1 for species abbreviations and Table 2 for skull measurement abbreviations.

R^2 = 0.53) and species pairs (all THSD: $P < 0.05$), except for *Chaetodipus penicillatus* and *C. baileyi* (P = 0.73) as well as *C. intermedius* and *C. californicus* (P = 0.44). All species range widely along PC2, which is little significant biologically (ANOVA: F = 1.58, P = 0.19, R^2 = 0.06).

The first 2 axes of the CVA represent over 65% of the variation (Figure 9A). Positive CV1 scores correspond to a larger IMW; negative scores correspond to a larger GCD. *Chaetodipus californicus* and *C. intermedius* occupy the positive end of the axis; *C. baileyi* and *C. hispidus* the negative end. Positive CV2 scores correspond to larger MANL, MAW, and MRD; negative CV2 scores correspond to larger GCL and GCW. *Chaetodipus baileyi* and *C. intermedius* occupy the negative end of CV2; *C. californicus*, *C. penicillatus* and *C. hispidus* the positive end of the axis. *Chaetodipus baileyi* (55.6%) and *C. hispidus* (68.8%) were classified correctly the least often. *Chaetodipus penicillatus* was correctly identified 77.3% of the time; *C. californicus* 71.4%. *Chaetodipus intermedius* was accurately identified most often (81.3% accuracy).

Dipodomys

The PCA of *Dipodomys* (Figure 7B) shows significant differences among species (MANOVA: F = 67.5, $P < 0.001$). The 2 significant axes explain over 41% of the variance in the dataset. PC1 is positively correlated with DMND, LDL, MANL, and MANW and negatively correlated with PW and IMW (Supplementary Data 4). *Dipodomys spectabilis*, *D. heermanni*, and *D. ingens* occupy the positive end of PC1; the other 3 species the negative end. The PC1 scores of the 6 species are significantly different (ANOVA: F = 123.8, $P < 0.001$, R^2 = 0.79). *Dipodomys ingens*, *D. ordii*, *D. heermanni*, *D. merriami*, and *D. spectabilis* are all statistically different (all THSD: $P <$ 0.001), excluding the pair *D. ordii* and *D. merriami* (P = 0.99). PC2 is positively correlated with GCL, GCW, and NL; it is negatively correlated with DM2. *Dipodomys deserti* occupies the positive end of PC2; all other species cluster on the lower end of the axis. *Dipodomys* species differ significantly in PC2 scores (ANOVA: F = 41.02, $P < 0.001$, R^2 = 0.56). Specifically, *Dipodomys deserti* differs significantly from all other species (all THSD: $P < 0.001$) and *D. ingens* from *D. heermanni* (P = 0.03). No other taxon pair is significantly different.

The first 2 axes of the CVA (Figure 9B) represent 83% of the variation. Positive CV1 scores correspond to larger GCL and MRD; negative CV1 scores correspond to larger MAW and MANL. *Dipodomys ordii* and *D. merriami* occupy the positive end of CV1; *D. spectabilis*, *D. ingens*, and *D. heermanni* the

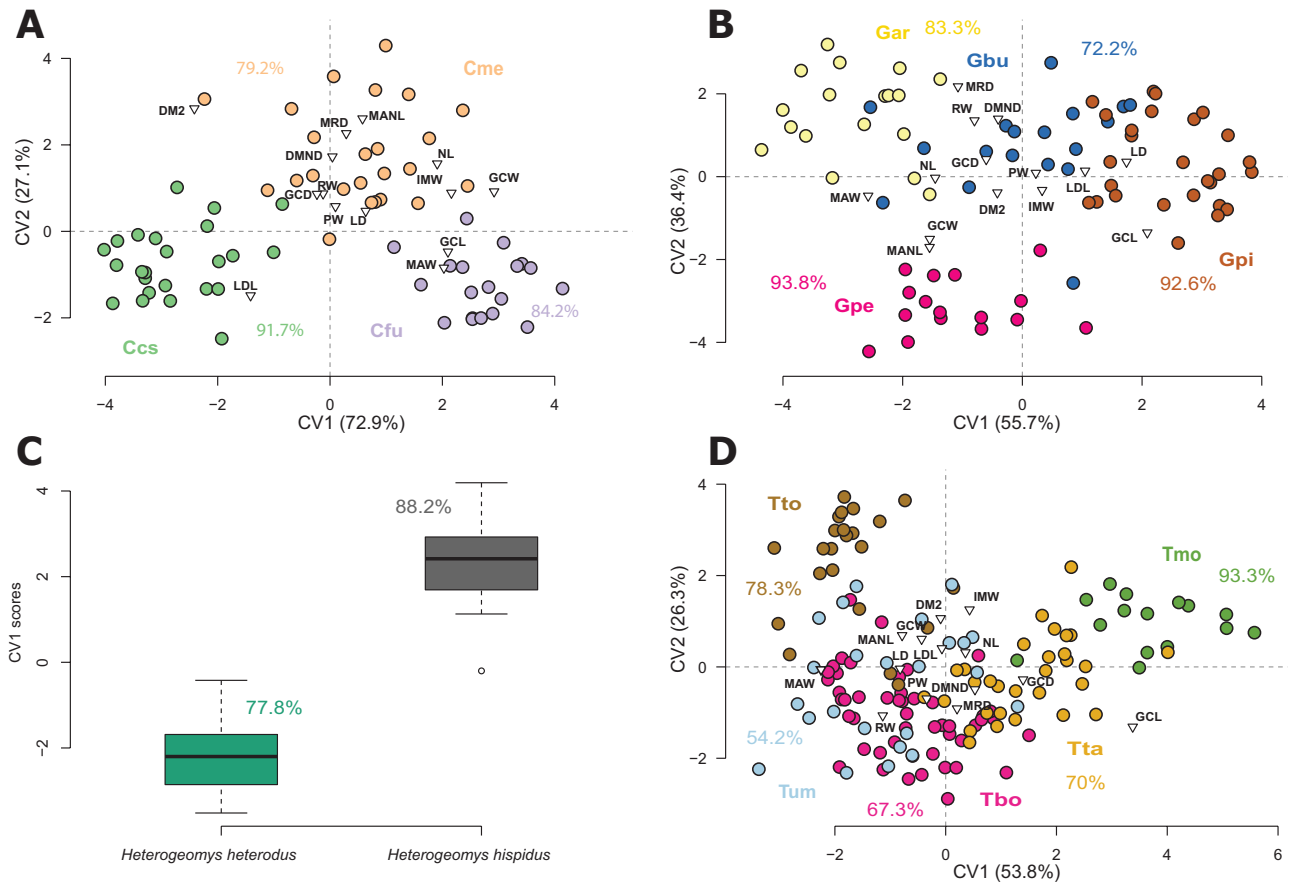

Figure 8. Canonical variate analyses at the species level. (A) *Cratogeomys*, (B) *Geomys*, (C) *Heterogeomys*, and (D) *Thomomys*. Each point represents a specimen. Species are color coded. See Table 1 for species abbreviations and Table 2 for skull measurement abbreviations.

negative end; *D. deserti* the middle of the axis. Positive CV2 scores correspond to a larger MANL in particular. Negative CV2 scores correspond to a larger GCW. *Dipodomys deserti* occupies the negative end of CV2; all other species have the positive end. *Dipodomys deserti* was accurately classified 100% of the time. *Dipodomys heermanni* was correctly identified over 91% of the time; *D. spectabilis* and *D. ingens* about 77% of the time; *D. merriami* and *D. ordii* 71% and 67% of the time, respectively.

Perognathus

The PCA of *Perognathus* (Figure 7C) shows significant differences among species (MANOVA: $F = 7.6$, $P < 0.001$). The first 2 of the 4 significant axes represent 38% of the variance in the dataset. PC1 is positively correlated with GCL, MANL, LD, and several other variables; it is negatively correlated with DMND (Supplementary Data 4). *Perognathus longimembris* and *P. parvus* occupy the positive end of PC1; *P. flavus* and *P. flavescens* the negative end. *Perognathus* species differ significantly in PC1 scores (ANOVA: $F = 27.01$, $P < 0.001$, $R^2 = 0.52$). *Perognathus flavescens* is significantly different in PC1 scores from all other species (THSD: $P < 0.001$); no other species pair is significantly different. PC2 is not biologically very informative (ANOVA: $F = 6.36$, $P < 0.001$; THSD: $P < 0.03$, $R^2 = 0.20$).

The first 2 axes of the CVA represent 92% of the variation (CV1: 49.4%, CV2: 43.3%). Positive CV1 scores correspond to larger IMW and LD; negative CV1 scores correspond to a larger GCD. *Perognathus parvus* occupies the center of CV1, *P. flavus* and *P. longimembris* the positive end, *P. flavescens* the negative end. Positive CV2 scores correspond to a larger NL, GCD, and MANL; negative CV2 scores correspond to a larger MAW. *Perognathus parvus* occupies the positive end of CV2. *Perognathus flavus*, *P. longimembris*, and *P. flavescens occupy* the negative end of the axis. *Perognathus flavus* and *P. longimembris* specimens were the most poorly identified (under 60% of the time). *Perognathus parvus* specimens were identified correctly 63% of the time. All specimens of *P. flavescens* were accurately classified.

Heteromys

The PCA of *Heteromys* (Figure 7D) shows significant differences among species (MANOVA: $F = 17.8$, $P < 0.001$). The 2 significant axes account for almost 47% of the variance in the dataset. PC1 is positively correlated with GCW, GCD, and several other variables; it is negatively correlated with MRD, MANL, LD, and LDL (Supplementary Data 4). *Heteromys pictus*, *H. gaumeri*, and *H. irroratus* occupy the positive end of the axis; the other 2 species the negative end. The PC1 scores of the 5 species are significantly different (ANOVA: $F = 27.5$, $P < 0.001$, $R^2 = 0.57$). Three of the 10 pairwise comparisons of PC1 scores between species are not significantly different: *H. pictus* and *H. irroratus* (THSD: $P = 0.06$), *H. irroratus* and *H. gaumeri* (THSD: $P = 1.00$), and *H. anomalus* and *H. desmarestianus* (THSD: $P = 0.70$). PC2 is positively correlated with DMND and negatively correlated with PW. *Heteromys gaumeri*, *H. desmarestianus*, and *H. anomalus* occupy the positive end of PC2; the other 2 species the

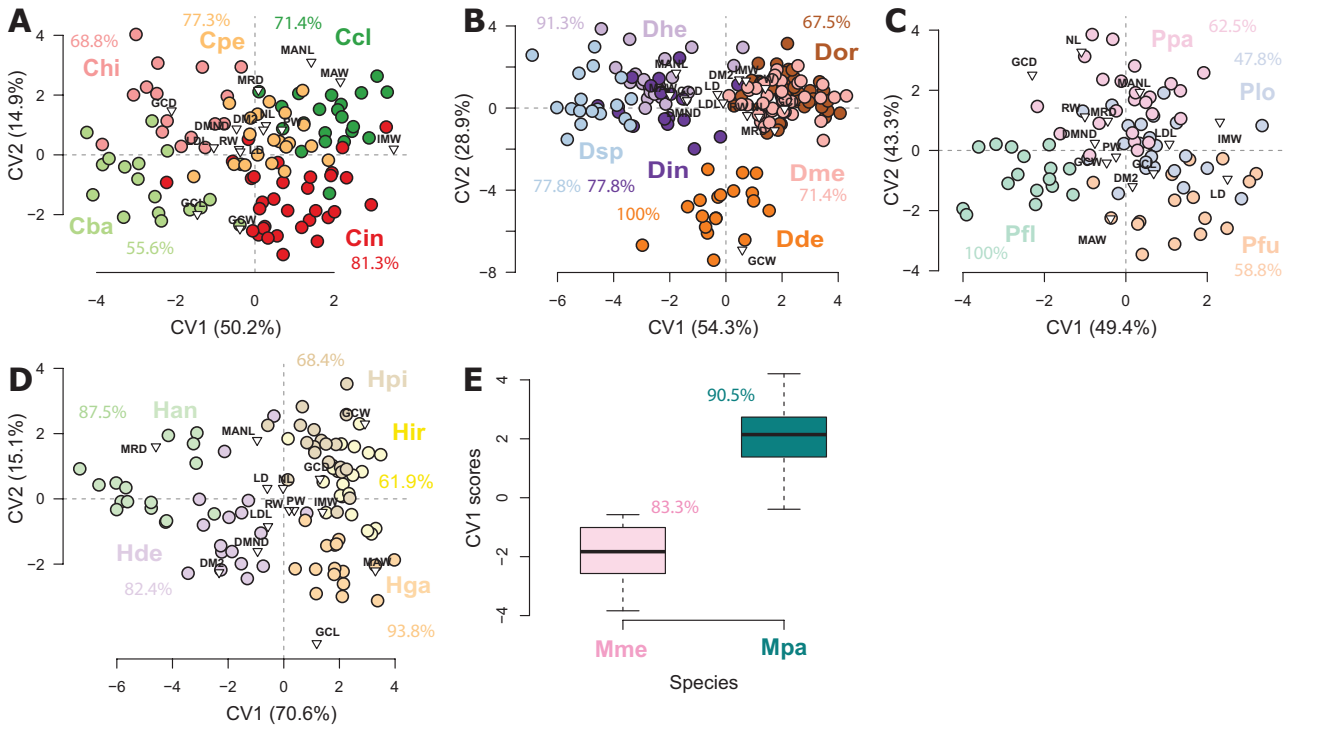

Figure 9. Canonical variate analyses at the species level. (A) *Chaetodipus*, (B) *Dipodomys*, (C) *Perognathus*, (D) *Heteromys*, and (E) *Microdipodops*. Each point represents a specimen. Species are color coded. See Table 1 for species abbreviations and Table 2 for skull measurement abbreviations.

negative end of the axis. The species are significantly different along PC2 (ANOVA: $F = 11.3$, $P < 0.001$, $R^2 = 0.35$). *Heteromys gaumeri* has significantly higher PC2 scores than all other species (THSD: $P < 0.001$ for all comparisons) except *H. desmarestianus*. *Heteromys pictus* has significantly lower PC2 scores than *H. desmarestianus* (THSD: $P = 0.007$).

CV1 represents 70.6% of the variation (Figure 9D). Positive scores correspond to larger MAW and GCW; negative scores correspond to a larger MRD. *Heteromys gaumeri*, *H. pictus*, and *H. irroratus* occupy the positive end of CV1; the other 2 species the negative end. CV2 represents 15.1% of the variation. Positive scores correspond to a larger GCW, MANL, and MRD; negative scores correspond to a larger GCL. *Heteromys pictus*, *H. anomalus*, and *H. irroratus* occupy the positive end of the axis; *H. desmarestianus* and *H. gaumeri* the negative end. *Heteromys gaumeri* was identified correctly most often, at 93.8%; *H. irroratus* the least, at 62%. *Heteromys pictus* was accurately identified 68.4% of the time; *H. anomalus* 87.5%; *H. desmarestianus* 82.4%.

Microdipodops

The PCA of *Microdipodops* (Figure 7E) shows significant differences among species (MANOVA: $F = 13.96$, $P < 0.001$). The 2 significant axes account for 44% of the variance in the dataset. The 2 species are not significantly different along PC1 (*t*-test: $t = 1.21$, $P = 0.24$). PC2 is positively correlated with MRD and NL; it is negatively correlated with GCD and several other variables. *Microdipodops pallidus* has significantly higher PC2 scores (*t*-test: $t = -4.8$, $P < 0.001$).

The CVA retains a single significant axis. Positive CV1 scores correspond to *M. pallidus* and negative CV1 scores to *M. megacephalus* (Figure 9E). *Microdipodops megacephalus* was accurately classified over 83% of the time; *M. pallidus* over 90% of the time.

Multivariate coefficient of variation

Both families display multivariate coefficient of variation (multiCV) values below 9% (Figure 10A). The multiCV is lower for Geomyidae (mean: 4.46%; median: 4.33%) than Heteromyidae (mean: 3.59%; median: 3.58%). The genus-level multiCVs show that all geomyid genera display greater variation in skull morphology than all heteromyid genera. Among geomyids, *Thomomys* has the highest multiCV (multiCV = 6.06%), *Heterogeomys* the lowest (multiCV = 4.73%). Within Heteromyidae, *Chaetodipus* displays the highest level of variation (multiCV = 4.52%), *Dipodomys* the lowest (multiCV = 3.58%). The standard deviation in multiCV differs little between the 2 families (Heteromyidae: 0.74, Geomyidae: 0.71). The species-level multiCV values of geomyids reveal a range of variation within all genera, except *Cratogeomys*. *Geomys personatus* displays the lowest amount of variation (Figure 10B). *Thomomys bottae* and *T. umbrinus* display the highest amount of variation. The species-level multiCV for heteromyids reveals that all species of *Dipodomys* show relatively low amounts of variation (Figure 10C); high levels of variation are present across all other genera. *Dipodomys merriami* displays the lowest amount of variation. *Chaetodipus baileyi* and *Perognathus longimembris* display the largest amount of variation. There is no significant relationship between taxon size and multiCV (PGLS: mean $t = 0.002$, mean $P = 0.617$).

Allometry

In Geomyidae, the regression between size and PC1 is negative ($R^2 = 0.24$, $P = 0.044$; Figure 11A) and positive for

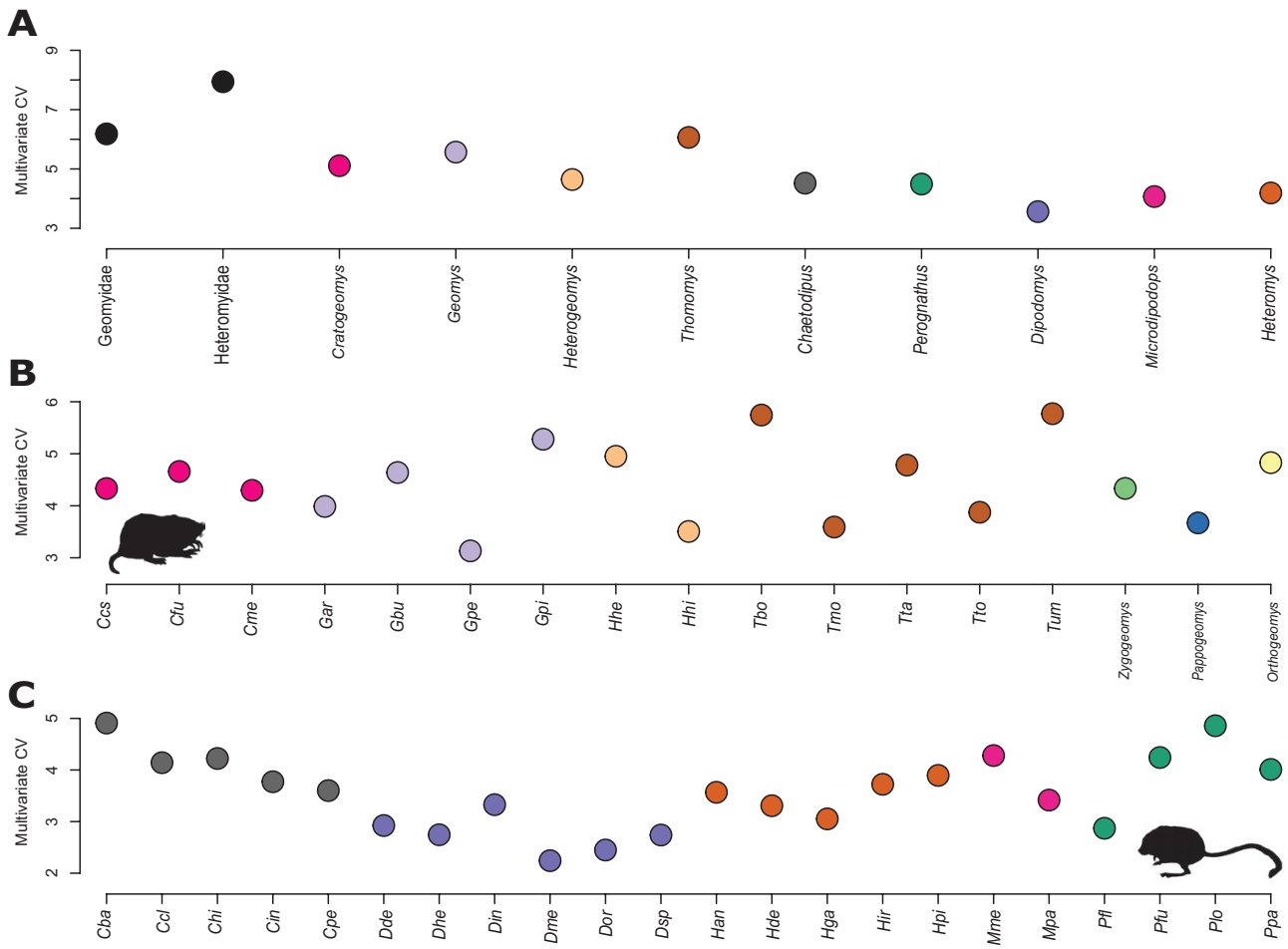

Figure 10. Multivariate coefficients of variation across taxonomic levels:. (A) family and genus-level coefficients; (B) species-level coefficients within Geomyidae; (C) species-level coefficients within Heteromyidae. Genera are color coded. Species abbreviations are provided in Table 1.

PC2 (R^2 = 0.67, P = 0; Figure 11B). In Heteromyidae, the regression is positive for PC1 (R^2 = 0.73, P = 0.006; Figure 11C), negative for PC2 (R^2 = 0.59, P = 0; Figure 11D). The subfamily Dipodomyinae displays a different allometric slope compared to perognathines and heteromyines (Figure 11C). When the 2 groups are considered independently, the allometric relationship is much stronger (Figure 11E,F). In both dipodomyines (R^2 = 0.92, P = 0) and non-dipodomyines (R^2 = 0.88, P = 0), the relationship between size and shape is positive.

Discussion

Our results show that most geomoyid taxa can be distinguished by their size. The greater size variation we observe in Geomyidae compared to Heteromyidae is consistent with prior, narrower, studies of size variation across pocket gophers (Hafner and Hafner 1988; Hafner et al. 2014). The higher prevalence of sexual size dimorphism in geomyids compared to heteromyids (Calede and Brown 2021) likely contributes to the greater size variation in Geomyidae, although there is no evidence that the species with the largest size variation in our analyses are also those with significant sexual size dimorphism (Calede and Brown 2021). The lack of size difference between *Heterogeomys* and *Orthogeomys* we recover is consistent with prior analyses (Spradling et al. 2016). Our finding that species of *Perognathus* are mostly smaller than those of the sister genus *Chaetodipus* is also consistent with previous research (Wyatt et al. 2021); the exact rank order of species and statistical differences differ somewhat between our analyses based on skull measurements and those of Wyatt et al. (2021) based on toothrow length. Future analyses building upon prior work on geomyoid body mass (Hopkins 2008) will be necessary to determine the best approach to quantifying size in pocket mice, and other geomyoids. At the species level, our results show that *H. heterodus* is larger than *H. hispidus*, but not significantly so, a pattern consistent with that of Spradling et al. (2016). Our data also show that many species of pocket mice can be differentiated using size. Wyatt et al. (2021) also found that toothrow size was an informative trait when identifying *Perognathus* and *Chaetodipus* specimens.

Our analyses demonstrate that the 2 geomyoid families can be reliably identified using skull shape, a result consistent with prior qualitative analyses (Hafner and Hafner 1988). Our phylomorphospace displays a clear association between the evolution of geomyids and the increase in the relative size of the lower jaw, and both diastemata as well as the deepening of the maxillary region and dentary. Our analyses also show that skull shape can be used to discriminate between geomyoid genera. Within Heteromyidae, species from the same genus are similar in shape. On the contrary, within Geomyidae, many species of a single genus

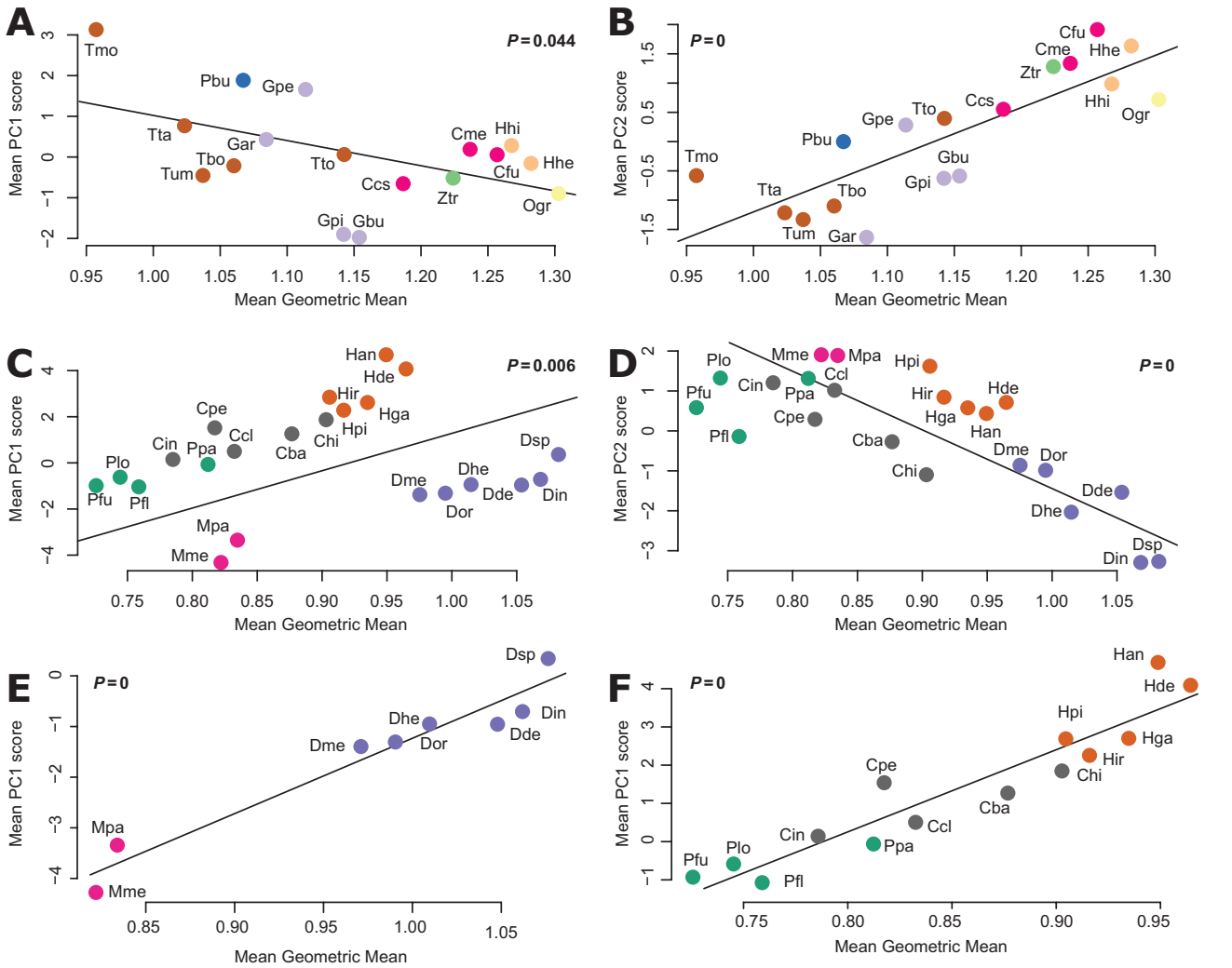

Figure 11. Allometric relationships within Geomyoidea. Allometric relationship between (A) size and PC1 scores within Geomyidae; (B) size and PC2 scores within Geomyidae; (C) size and PC1 scores within Heteromyidae; (D) size and PC2 scores within Heteromyidae; (E) size and PC1 scores within Dipodomyinae; And (F) size and PC1 scores within non-dipodomyine heteromyids. *P* values are provided for each relationship. Each point represents a species. Genera are color coded. Species abbreviations are provided in Table 1.

are scattered in morphospace and can closely resemble species from different genera. This pattern is suggestive of widespread morphological convergence and consistent with prior observations that geomyids greatly resemble one another in shape (Hafner and Hafner 1988) and that Geomyidae display low levels of skull divergence (Wahlert 1985). Wahlert (1985, p. 17) suggested that "either recent diversification or long conservation of a successful design after a period of rapid evolution" was responsible for this pattern of morphological similarity. Our results demonstrate that the ancestral geomyid morphology is highly apomorphic and divergent from the ancestral heteromyid morphology. Further testing of the competing hypotheses of Wahlert (1985) will require the analysis of morphological evolution in a time-calibrated phylogenetic framework that includes fossil species.

The greater morphological disparity within Heteromyidae reflects variation in the relative width of the skull in the rostral, zygomatic, and basicranial regions. No extant geomyids occupy the region of the morphospace that corresponds to skulls with narrow basicranial and zygomatic regions but broad rostra. This may be a product of extinction, but it could also be the consequence of the evolution of fossoriality. The effect of extinction could be tested by adding fossil gophers to the dataset, which could increase the morphospace occupation by geomyids, with some species occupying its lower half. Thus, although they do not have broad rostra, entoptychine gophers have narrower crania than their geomyine relatives (Calede and Rasmussen 2020). In fact, a prior ecomorphological analysis of skull shape in select fossil geomyids show that entoptychine and geomyine gophers can differ greatly in skull shape (Calede et al. 2019). Some fossil species of extant geomyid genera, particularly *Geomys garbanii*, also display skull morphologies that are divergent from those observed in congeners (White and Downs 1961; Calede et al. 2019). The association of the evolution of fossoriality and changes in skull morphology across subterranean rodent groups should be rigorously explored in a phylogenetic framework, but existing data already show that there is a strong association between broad zygomatic arches and burrowing (Hopkins and Davis 2009) as well as broad basicrania and burrowing (Hopkins 2005; Calede et al. 2019; Scarpitti and Calede 2022). Broad rostra are documented in other fossorial taxa, particularly head-lift diggers (e.g. Mylagaulidae; Hopkins

2005), but no extant or extinct geomyid has been determined to use head-lifting in burrowing.

Our phylomorphospace shows that the skull shape of the most recent common ancestor of all geomyoids resembled that of the most recent common ancestor of heteromyids (as opposed to that of geomyids) and specifically was most similar to *Chaetodipus* and *Perognathus*. As such, our results support the hypothesis that pocket mice represent a morphology similar to that of the most recent common ancestor of Geomyoidea (see Hafner and Hafner 1988). The future inclusion of fossil geomyoids into the framework we present here will enable a test of the accuracy of these ancestral character state constructions.

Although we do recover some similarities (mainly the relatively narrow rostrum of *Geomys* compared to *Thomomys*, *Cratogeomys*, and *Heterogeomys*), our results of the genus-level morphological variation within Geomyidae do not mirror prior findings of a clear segregation between claw-digging and tooth-digging taxa based on a smaller (and slightly different) set of measurements (Lessa and Stein 1992). For example, *Zygogeomys*, a scratch-digging taxon (Hopkins and Davis 2009), and *T. bottae*, a chisel tooth–digging animal (Hopkins and Davis 2009), are found to have very similar morphologies in our analyses. In that regard, our results are similar to those of Samuels and Van Valkenburgh (2008: Fig. 2) who found strong morphological similarities among the 4 geomyid species they studied notwithstanding digging mode. However, we did not measure some traits that are likely associated with burrowing in chisel tooth–digging gophers (e.g. upper incisor procumbency and bite force; Lessa and Thaeler 1989; Kalthoff and Mörs 2021). A more complete picture of the link between evolutionary morphology and ecology in this family will require the inclusion of these measurements as well as fossil taxa. Indeed, one would expect higher bite force and greater incisor procumbency in chisel tooth–digging species (Marcy et al. 2016; Kalthoff and Mörs 2021).

It appears from our findings that ecomorphological adaptations concentrated in the incisors (such as procumbency and incisor shape) may not require major rearrangements in cranial morphology across geomyid genera. That is apparently not true within *Thomomys*. Indeed, within this genus, we recover a similar pattern of convergence in cranial morphology between *T. talpoides* and *T. bottae* that was documented by Marcy et al. (2016) that supports the conclusion that changes in cranial morphology were critical to the evolution of chisel tooth digging. Additionally, data from our size analysis also show that size increases in these 2 species could have played a role in their adaptation to chisel tooth digging alike Marcy et al. (2016). The scaling of procumbency and bite force with size in geomyids should be rigorously investigated to further test these hypotheses across a broad sample of taxa.

We do find morphological differences between dolichocephalic gophers (e.g. *Orthogeomys* and *Heterogeomys*) and so-called generalized ones (e.g. *Geomys*, *Pappogeomys*, *C. castanops*, and *C. merriami*; Wilkins and Woods 1983). In a prior analysis restricted to the 2 genera, *Orthogeomys* and *Heterogeomys* occupied different regions of the morphospace, in part as a consequence of differences in interorbital constriction, a variable we did not measure (Spradling et al. 2016). Our CVAs show that most geomyoid genera can accurately (>75%) be identified using skull measurements. Only *Orthogeomys*, *Geomys*, and *Pappogeomys* are difficult to identify from skull measurements. The lower rate of accurate classification for *Orthogeomys* is a consequence of its similarity with *Heterogeomys* in the absence of data on interorbital constriction. The low rates for *Pappogeomys* and *Geomys* are associated with the convergence between these 2 genera, particularly between *P. bulleri* and *G. personatus*. *Pappogeomys* has historically been difficult to delineate systematically in the absence of molecular data (Hafner et al. 2009). Tooth shape appears to be more informative than skull morphology in identifying *Geomys*, *Orthogeomys*, *Heterogeomys*, and *Thomomys*, but not *Cratogeomys* (Calede and Glusman 2017). Tooth shape outperforms skull morphology in distinguishing between perognathine genera (Wyatt et al. 2021).

Our analyses demonstrate that geomyid species can reliably be identified using skull morphology. Indeed, major morphological differences among species within each genus can be observed (Figure 6) and inform taxonomic identification (Figure 8). Skull morphology is highly informative of taxonomic identity within *Cratogeomys*. This result is consistent with prior analyses of skull shape in the genus (Hafner et al. 2005, 2008). All *Cratogeomys* specimens can be identified accurately over 79% of the time. These rates of classification are overall higher than those found using dental morphology (Calede and Glusman 2017). The pattern of overlap we observe within *Geomys* is similar to the one described by Mauk et al. (1999), although *G. pinetis* was not included in their analyses. The overlap of *G. bursarius* with both *G. pinetis* and *G. arenarius* explains the lower correct identification percentage for this taxon (72.2%) compared to the other species of the genus, which can all reliably be identified using skull measurements. The high rates of accurate classification for *G. pinetis* using skull measurements mirror the results of an analysis using tooth shape (Calede and Glusman 2017). Another taxon, *G. arenarius*, is more easily identified using skull measurements than tooth shape. Within *Heterogeomys*, there is little overlap in morphology between the 2 species. Although *H. hispidus* is more often accurately classified, both species can be reliably identified using skull measurements. Spradling et al. (2016) found *H. heterodus* to be more often correctly identified than *H. hispidus* with a different set of craniodental measurements, but Calede and Glusman (2017) found similar rates of correct classification using dental morphology. Our findings are consistent with the validity of skull measurements as a taxonomic tool in this genus. Within *Thomomys*, the 2 subgenera (*Thomomys* and *Megascapheus*) overlap in cranial shape, more so than in the analyses of Marcy et al. (2016) in which only females were included. Further, overlaps in morphology of *T. bottae* with essentially all other species lead to a low rate of correct classification for the taxon (67.3%); this same species was also difficult to differentiate from others using dental morphology (Calede and Glusman 2017). The wide morphospace occupation of *T. umbrinus*, with 2 clusters of specimens, leads to the low rate of accurate identification for this species. Prior analyses of the morphospace occupation of *T. umbrinus* specimens have showed the presence of morphologically divergent subspecies (Calede and Brown 2021), and a detailed analysis of the species demonstrates the presence of morphological variance across populations and subspecies of the taxon (Mathis et al. 2014). Future analyses including large samples of subspecies of *T. umbrinus* as well as other sympatric and parapatric *Thomomys* species will help determine the potential for skull morphology to help resolve the identification of uncertain specimens in museums. *Thomomy monticola* and

T. townsendii, 2 taxa with low morphological disparity, can reliably be identified using skull measurements, better so than using tooth morphology (Calede and Glusman 2017).

The skull morphology of heteromyids (Figure 7) can be used to inform species-level taxonomic identification (Figure 9), although not as well as in geomyids (54% vs. 59% of species 75% accurately identified or better). Within *Chaetodipus*, there is a lot of overlap in morphospace among species. Variation within *C. intermedius* is driven largely by RW, greater cranial length, mandible length, greater cranial depth, and mandible length. These are all very important variables in the analysis of intraspecific variability of skull measurements (Weckerly and Best 1985). Our results suggest that these variables are also important in driving the intraspecific variation within *C. hispidus* and *C. penicillatus*. The rates of classification for the species are low in 3 of the 5 taxa (*C. hispidus*, *C. baileyi*, and *C. californicus*), but this is a consequence of single outliers in each species that suggest that larger sample sizes for all taxa, which help capture more of the morphological variation across populations, would help improve these classification rates. *Chaetodipus intermedius* and *C. penicillatus* can be reliably identified from skull measurements. Interestingly, *C. intermedius* is also one of the species of the genus with the most distinctive dental morphology (Wyatt et al. 2021). *Chaetodipus penicillatus* is not and *C. hispidus* is, however, suggesting a lack of association between morphological divergences in the dentition and the cranium. Within *Dipodomys*, there is a lot of overlap in morphospace among clusters of species. *Dipodomys deserti* is distinct in morphology from all other species of the genus, largely because of a relatively larger cranium (including length and width); it can be reliably identified from skull measurements, better so than using tooth morphology (Carrasco 2000). *Dipodomys merriami* and *D. ordii* as well as *D. ingens*, *D. heermanni*, and *D. spectabilis* are very similar in morphology. As a consequence, the rates of classification are low for 2 of these taxa (*D. merriami* and *D. ordii*) for which dental morphology is more useful (Carrasco 2000). Within *Perognathus*, there is a lot of overlap in morphospace between *P. longimembris* and *P. flavus*; it is largely driven by similarities in rostral and maxillary morphology. These variables are also important in driving the intraspecific variation within *P. longimembris* and *P. flavus*. Prior analyses of the variation within *P. parvus* failed to recover particular morphological variables as indicative of populations (Riddle et al. 2014). The rates of classification are low in 3 of the 4 taxa (*P. flavus*, *P. longimembris*, and *P. parvus*), which overlap greatly in morphospace, and very high for *P. flavescens*. A similar pattern of morphological overlap and high misidentification rates was recovered in the tooth shape analysis of Wyatt et al. (2021). *Heteromys pictus* and *H. irroratus*, 2 species that display important intraspecific variation, overlap one another heavily in morphospace and show low rates of classification. *Heteromys desmarestianus*, *H. gaumeri*, and *H. anomalus*, however, can reliably be identified from skull measurements. There are 2 clusters of specimens within *H. desmarestianus*, which suggests that future analyses of the intraspecific variation within this species may reveal interesting taxonomic information. Prior studies of the variation in skull shape within *Heteromys* have contributed to the identification of several species (Anderson and Jarrín-V 2002; Anderson and Timm 2006; Anderson and Gutierrez 2009). Within *Microdipodops*, the separation in morphospace between the 2 species is a consequence of the longer and deeper rostrum of *M. pallidus* and the longer diastemata as well as deeper maxilla and basicranium of *M. megacephalus*. *Microdipodops pallidus* specimens are identified correctly more often than *M. megacephalus* specimens, but the rates of classification for both species are high. The variable and complimentary powers of skull and tooth morphologies in identifying geomyoid taxa suggest that a combined approach including both elements of the craniomandibular apparatus could be a powerful tool in identifying phenotypically similar species, cryptic species, and recently extinct taxa within difficult-to-identify taxa like *Perognathus*.

Our analysis of morphological disparity using the multiCV shows that Heteromyidae displays greater variation than Geomyidae. This is consistent with the morphospace occupation observed in the phylomorphospace and prior observations (Hafner and Hafner 1988). It may reflect a canalization of morphology associated with burrowing evolution. Thus, the absence of geomyids with low MAW may be a consequence of the muscular attachments on the zygomatic arch associated with burrowing (Hopkins and Davis 2009). Similarly, the absence of geomyids with narrow basicrania likely reflects adaptations to burrowing of the occipital bone (Scarpitti and Calede 2022). Contrary to the family-level analysis, the multiCVs of geomyid genera tend to be larger than those of heteromyid genera. Unlike for dental morphology (Calede and Glusman 2017), *Thomomys* does not display lower disparity in skull morphology than Geomyini genera. The range of squared multiCVs we recover across geomyoid species is narrower than that found across populations of *T. bottae* (Soulé and Zegers 1996). None of the species we studied reach the highest level of morphological variation observed by Soulé and Zegers (1996). Nonetheless, *T. bottae* displays the second highest level of variation of any geomyid (or even geomyoid) species we studied, after *T. umbrinus*. On the contrary, *T. monticola* and *T. townsendii* display very low levels of multivariate variation. Thus, *Thomomys* shows the highest range of multiCV values among species of any geomyoid genus; *Cratogeomys* shows the lowest level. There are a few outlier species that display unexpected levels of variation for the genus. *Geomys personatus* has a very low multiCV compared to congenerics; the same is true for *P. flavescens*. Future analyses exploring the correlation between morphological and genetic variation in geomyoids (following Soulé and Zegers 1996) may shed new lights on the taxonomy of the family, particularly with regards to cryptic taxonomy in geographically widespread and highly phenotypically variable taxa, and the effects of possible bottlenecks on phenotype in species that are little variable.

Notable morphological variables that scale with negative allometry within Geomyidae include IMW, GCD, DMND, PW, and GCL, whereas the variables that scale with positive allometry include LDL, LD, MRD, and GCW. The relative positions of *T. monticola*, *T. talpoides*, *T. bottae*, and *T. townsendii* in our analysis mirror those recovered by Marcy et al. (2016) in their analysis of the cranium of the genus, particularly the analysis of the ventral view of the skull. Within Heteromyidae, the morphological variables that scale with negative allometry include GCD, GCW, PW, MAW, and LDL, whereas the variables that scale with positive allometry include MANL, GCL, RW, LD, NL, and MRD. Both families share common allometric patterns for 4 morphological variables (PW, GCD, LD, and MRD), which may be inherited from the common ancestor for the 2 families. In the case of NL (in heteromyids

only) and LD (in both families), the pattern of elongation of these features with body size corresponds to a positive craniofacial evolutionary allometry that has been documented extensively in placentals broadly (Cardini 2019) and rodents specifically (Marcy et al. 2020; Alhajeri 2021, 2022). Two of the variables associated with the extreme inflation of the bullae of dipodomyines (GCD and GCW, but not GCL) scale with negative allometry. The allometric difference in slope between dipodomyines and non-dipodomyines supports an important role of heterochrony in the evolution of the morphology of the subfamily (Hafner and Hafner 1988). The exact importance of heterochrony in driving skull evolution within Heteromyidae should be further explored by incorporating fossil dipodomyines in the framework we present herein (Wood 1935; Voorhies 1975). This will enable the specific test of the hypothesis that Dipodomyinae is pedomorphic and geomyids are hypermorphic as suggested by Hafner and Hafner (1988) and supported in part by our analyses so far.

The framework presented herein should be used to investigate the disparity of skull morphologies observed in the geomyoid fossil record. In fact, fossils will enable formal tests of several hypotheses of skull evolution in Geomyoidea combined with analyses of rate of morphological evolution. Future work incorporating juvenile morphology will also be important to rigorously test developmental hypotheses.

Acknowledgments

Meg Daly and Grant Terrell (OSUM), John Wible and Suzanne McLaren (CM), Darrin Lunde (USNM), Marisa Surovy (AMNH), Roberta Muelheim (CMNH), Jim Dines (LACM), Verity Mathis (UF), and C. William Kilpatrick (UVM) provided access to specimens and records. We thank the University of California Berkeley Museum of Vertebrate Zoology (MVZ) for use of their specimen images and CalPhotos for access and use of their digital resources. We thank the USNM and UF for access and use of specimen photos. Space at OSUM was provided to the Calede lab by Rachelle Adams and Bryan Carstens. Sam Hopkins and Sam Price provided their tree file. Andrew Brown, Erica Scarpitti, Anas Tantash, and Madeline Ball assisted with data collection. Charity Gottfried and Katlyn Large collaborated on an initial iteration of this project. Ryan Norris and 4 anonymous reviewers provided feedback on earlier versions of this manuscript. The silhouette of the pocket gopher used in the figures is from phylopic (Public Domain Dedication 1.0 licence).

Funding

This research was funded by a Paleontological Society Norman Newel Award, a College of Arts and Sciences Regional Campus Research and Creative Activity Grant from the Ohio State University, a research grant from the Ohio State University at Marion, startup funds from the Ohio State University to JC, and Summer Research Assistantship funds from the Ohio State University at Marion to LN. Some of the ideas for this project were developed while JC was supported by a Meaningful Inquiry grant from The Ohio State University library system.

Conflict of interest

The authors declare no conflict of interest.

Author contributions

JC developed the data collection protocol. LN and JC collected data, LN and JC analyzed the data, LN wrote the manuscript, LN and JC edited and approved the manuscript.

References

Alexander LF, Riddle BR, 2005. Phylogenetics of the new world rodent family Heteromyidae. *J Mammal* **86**:366–379.

Alhajeri BH, 2021. A morphometric comparison of the cranial shapes of Asian dwarf hamsters (*Phodopus*, Cricetinae, Rodentia). *Zool Anz* **292**:184–196.

Alhajeri BH, 2022. Geometric differences between the crania of Australian hopping mice (*Notomys*, Murinae, Rodentia). *Aust Mammal* **44**:24–38.

Anderson RP, 2003. Taxonomy, distribution, and natural history of the genus *Heteromys* (Rodentia: Heteromyidae) in western Venezuela, with the description of a dwarf species from the Península de Paraguaná. *Am Mus Novit* **3396**:1–43.

Anderson RP, Gutiérrez EE, 2009. Taxonomy, distribution, and natural history of the genus *Heteromys* (Rodentia: Heteromyidae) in central and eastern Venezuela, with the description of a new species from the Cordillera de la Costa. In: Voss RS, Carleton MD, editors. *Systematic Mammalogy: Contributions in Honor of Guy G. Musser*, Vol. **331**. New York City (NY): Bulletin of the American Museum of Natural History, 33–93.

Anderson RP, Jarrín VP, 2002. A new species of spiny pocket mouse (Heteromyidae: *Heteromys*) endemic to western Ecuador. *Am Mus Novit* **3382**:1–26.

Anderson RP, Timm RM, 2006. A new species of spiny pocket mouse (Rodentia: Heteromyidae: *Heteromys*) from Northwestern Costa Rica. *Am Mus Novit* **3509**:1–38.

Anderson RP, Weksler M, Rogers DS, 2006. Phylogenetic analyses of spiny pocket mice (Heteromyidae: Heteromyinae) based on allozymic and morphological data. *J Mammal* **87**:1218–1233.

Baker RJ, Williams SL, 1974. *Geomys tropicalis*. *Mamm Species* **35**:1–4.

Bartholomew GA, Cary GR, 1954. Locomotion in pocket mice. *J Mammal* **35**:386–392.

Bartholomew GA, Caswell HH, 1951. Locomotion in kangaroo rats and its adaptive significance. *J Mammal* **32**:155–169.

Belfiore NM, Lui L, Moritz C, 2008. Multilocus phylogenetics of a rapid radiation in the genus *Thomomys* (Rodentia: Geomyidae). *Syst Biol* **57**:294–310.

Braun JK, Coyner BS, Mares MA, 2021. Modern extirpation of the Texas kangaroo rat, *Dipodomys elator*, in Oklahoma: Changing land use and climate over a century of time as the road to eventual extinction. *THERYA* **12**:177–186.

Calede JJM, Brown A, 2021. Sexual dimorphism in cranial shape and size in geomyoid rodents: Multivariate and evolutionary perspectives. *Curr Zool* **67**:1–18.

Calede JJM, Glusman JW, 2017. Geometric morphometric analyses of worn cheek teeth help identify extant and extinct gophers (Rodentia, Geomyidae). *Palaeontology* **60**:281–307.

Calede JJM, Rasmussen DL, 2020. New gophers (Rodentia: Geomyidae) from the Cabbage Patch beds of Montana (Renova Formation) and the phylogenetic relationships within Entoptychinae. *Ann Carnegie Mus* **86**:107–167.

Calede JJM, Samuels JX, Chen M, 2019. Locomotory adaptations in entoptychine gophers (Rodentia: Geomyidae) and the mosaic evolution of fossoriality. *J Morphol* **280**:879–907.

Cardini A, 2019. Craniofacial allometry is a rule in evolutionary radiations of placentals. *Evol Biol* **46**:239–248.

Carrasco MA, 2000. Species discrimination and morphological relationships of kangaroo rats (*Dipodomys*) based on their dentition. *J Mammal* **81**:107–122.

Cervantes FA, 2021. The tropical pocket gopher *Geomys tropicalis* on the brink of extinction. *THERYA Notes* **2**:1–7.

Connior MB, 2011. *Geomys bursarius* (Rodentia: Geomyidae). *Mamm Species* **43**:104–117.

Desha PG, 1967. Variation in a population of kangaroo rats, *Dipodomys ordii medius* (Rodentia: Heteromyidae) from the high plains of Texas. *Southwest Nat* 12:275–289.
D'Elía G, Fabre P-H, Lessa EP, 2019. Rodent systematics in an age of discovery: Recent advances and prospects. *J Mammal* **100**:852–887.
Demastes JW, Spradling TA, Hafner MS, Hafner DJ, Reed DL, 2002. Systematics and phylogeography of pocket gophers in the genera *Cratogeomys* and *Pappogeomys*. *Mol Phylogenet Evol* **22**:144–154.
Djawdan M, 1993. Locomotor performance of bipedal and quadrupedal heteromyid rodents. *Funct Ecol* **7**:195–202.
Fabre P-H, Hautier L, Dimitrov D, Douzery EJP, 2012. A glimpse on the pattern of rodent diversification: A phylogenetic approach. *BMC Evol Biol* **12**:88.
Gutiérrez-Costa MA, Gonzaléz-Cózatl FX, Ramírez-Martínez MM, Iñiguez-Dávalos LI, Rogers DS, 2021. Molecular data suggest that *Heteromys irroratus bulleri* should be recognized as a species-level taxon. *THERYA* **12**:139–148.
Hafner MS, Gates AR, Mathis VL, Demastes JW, Hafner DJ, 2011. Redescription of the pocket gopher *Thomomys atrovarius* from the Pacific coast of mainland Mexico. *J Mammal* **92**:1367–1382.
Hafner DJ, Gonzales EE, Demastes JW, Spradling TA, Cervantes FA, 2014. Rediscovery of the pocket gopher *Orthogeomys lanius* (Rodentia: Geomyidae) in Veracruz, Mexico. *J Mammal* **95**:792–802.
Hafner JC, Hafner MS, 1988. Heterochrony in rodents. In: McKinney ML editor. *Heterochronyin Evolution*. New York, NY, USA: Plenum Publishing Corporation, 217–235.
Hafner DJ, Hafner MS, Hasty GL, Spradling TA, Demastes JW, 2008. Evolutionary relationships of pocket gophers (*Cratogeomys castanops* species group) of the Mexican Altiplano. *J Mammal* **89**:190–208.
Hafner MS, Hafner DJ, Demastes JW, Hasty GL, Light JE, et al., 2009. Evolutionary relationships of pocket gophers of the genus Pappogeomys (Rodentia: Geomyidae). *J Mammal* **90**:47–56.
Hafner MS, Light JE, Hafner DJ, Brant SV, Spradling TA et al., 2005. Cryptic species in the Mexican pocket gopher *Cratogeomys merriami*. *J Mammal* **86**:1095–1108.
Hafner JC, Light JE, Hafner DJ, Hafner MS, Reddington E et al., 2007. Basal clades and molecular systematics of heteromyid rodents. *J Mammal* **88**:1129–1145.
Hafner MS, Spradling TA, Light JE, Hafner DJ, Demboski JR, 2004. Systematic revision of pocket gophers of the *Cratogeomys gymnurus* species group. *J Mammal* **85**:1170–1183.
Hopkins SSB, 2005. The evolution of fossoriality and the adaptive role of honrs in the Mylagaulidae (Mammalia: Rodentia). *Proc R Soc B* **272**:1705–1713.
Hopkins SSB, 2008. Reassessing the mass of exceptionally large rodents using toothrow length and area as proxies for body mass. *J Mammal* **89**:232–243.
Hopkins SSB, Davis EB, 2009. Quantitative morphological proxies for fossoriality in small mammals. *J Mammal* **90**:1449–1460.
Jones CA, Baxter CN, 2004. *Thomomys bottae*. *ASM* **742**:1–14.
Jungers WL, Falsetti AB, Wall CE, 1995. Shape, relative size, and size-adjustments in morphometrics. *Yearb Phys Anthropol* **38**:137–161.
Kalthoff DC, Mörs T, 2021. Biomechanical adaptations for burrowing in the incisor enamel microstructure of Geomyidae and Heteromyidae (Rodentia: Geomyoidea). *Ecol Evol*. doi:10.1002/ece3.7765
Kays R, Lasky M, Allen ML, Dowler RC, Hawkins MTR et al., 2022. Which mammals can be identified from camera traps and crowd-sourced photographs? *J Mammal*. doi:10.1093/jmammal/gyac021
Lal KK, Gupta BK, Punia P, Mohindra V, Saini VS et al., 2015. Revision of gonius subgroup of the genus *Labeo* Cuvier, 1816 and confirmation of species status of *Labeo rajasthanicus* (Cypriniformes: Cyprinidae) with designation of a neotype. *Indian J Fish* **62**:10–22.
Lessa EP, Stein BR, 1992. Morphological constraints in the digging apparatus of pocket gophers (Mammalia: Geomyidae). *Biol J Linn Soc* **47**:439–453.
Lessa EP, Thaeler CS, 1989. A reassessment of morphological specializations for digging in pocket gophers. *J Mammal* **70**:689–700.
Madar SI, Rose MD, Kelley J, MacLatchy L, Pilbeam D, 2002. New *Sivapithecus* postcranial specimens from the Siwaliks of Pakistan. *J Hum Evol* **42**:705–752.
Mammal Diversity Database, 2021. *Mammal Diversity Database (Version 1.7)*. *Zenodo*. Available from: https://zenodo.org/record/5651212#.YeBlTf7MLIU
Marcy AE, Guillerme T, Sherratt E, Rowe KC, Phillips MJ et al., 2020. Australian rodents reveal conserved cranial evolutionary allometry across 10 million years of murid evolution. *Am Nat* **196**:755–768.
Marcy AE, Hadly EA, Sherratt E, Garland K, Weisbecker V, 2016. Getting a head in hard soils: Convergent skull evolution and divergent allometric patterns explain shape variation in a highly diverse genus of pocket gophers (*Thomomys*). *BMC Evol Biol* **16**:1–16.
Martínez-Gallardo R, Sánchez-Cordero V, 1993. Dietary value of fruits and seeds to spiny pocket mice, *Heteromys desmarestianus* (Heteromyidae). *J Mammal* **74**:436–442.
Mathis VL, Hafner MS, Hafner DJ, 2014. Evolution and phylogeography of the *Thomomys umbrinus* species complex (Rodentia: Geomyidae). *J Mammal* **95**:754–771.
Mauk CL, Houck MA, Bradley RD, 1999. Morphometric analysis of seven species of pocket gophers (*Geomys*). *J Mammal* **80**:499–511.
McGarigal K, 2015. *Biostats*. Available from: http://www.umass.edu/landeco/teaching/ecodata/labs/biostats.R.
Orme D, 2018. *The caper package: comparative analysis of phylogenetics and evolution in R*. Available from: https://CRAN.R-project.org/package=caper.
Ortiz-Caballero E, Jiménez-Hidalgo E, Bravo-Cuevas VM, 2020. A new species of the gopher *Gregorymys* (Rodentia, Geomyidae) from the early Oligocene (Arikareean 1) of southern Mexico. *J Paleo* **94**:1191–1201.
Paradis E, Claude J, Strimmer K, 2004. APE: Analyses of phylogenetics and evolution in R language. *Bioinformatics* **20**:289–290.
Parsons EI, Gitzen RA, Pynne JT, Conner LM, Castleberry SB et al., 2022. Determining habitat requirements for the southeastern pocket gopher *Geomys pinetis* at multiple scales. *J Mammal*. doi:10.1093/jmammal/gyab144
Price SA, Hopkins SSB, 2015. The macroevolutionary relationship between diet and body mass across mammals. *Biol J Linn Soc* **115**:173–184.
R Core Team, 2019. *R: A Language and Environment for Statistical Computing*. Vienna (Austria): R Foundation for Statistical Computing.
Revell LJ, 2012. phytools: An R package for phylogenetic comparative biology (and other things). *Methods Ecol Evol* **3**:217–223.
Riddle BR, Jezkova T, Eckstut ME, Oláh-Hemmings V, Carraway LN, 2014. Cryptic divergence and revised species taxonomy within the Great Basin pocket mouse *Perognathus parvus* (Peale, 1848) species group. *J Mammal* **95**:9–25.
Russell RJ, 1968. Evolution and classification of the pocket gophers of the subfamily Geomyinae. *Mus Nat Hist* **16**:473–579.
Samuels JX, 2009. Cranial morphology and dietary habits of rodents. *Zool J Linn Soc-Lond* **156**:864–888.
Samuels JX, Van Valkenburgh B, 2008. Skeletal indicators of locomotor adaptations in living and extinct rodents. *J Morphol* **269**:1387–1411.
Scarpitti EA, Calede JJM, 2022. Ecological correlates of the morphology of the auditory bulla in rodents: Application to the fossil record. *J Anat*. **240**:647–668.
Schneider CA, Rasband WS, Eliceiri KW, 2012. NIH Image to ImageJ: 25 years of image analysis. *Nat Methods* **9**:671–675.
Sidlauskas B, 2008. Continuous and arrested morphological diversification in sister clades of characiform fishes: A phylomorphospace approach. *Evolution* **62**:3135–3156.
Soulé ME, Zegers GP, 1996. Phenetics of natural populations. V. Genetic correlates of phenotypic variation in the pocket gopher *Thomomys bottae* in California. *J Hered* **87**:341–350.
Spradling TA, Demastes JW, Hafner DJ, Milbach PL, Cervantes FA et al., 2016. Systematic revision of the pocket gopher genus *Orthogeomys*. *J Mammal* **97**:405–423.
Strauss RE, 2010. Discriminating groups of organisms. *Lect Notes Earth Sci* **124**:73–91.
Taylor DS, Frank J, Southworth D, 2009. Mycophagy in Botta's pocket gopher *Thomomys bottae* in southern Oregon. *Northwest Sci* **83**:367–370.

Upham NS, Esselstyn JA, Jetz W, 2019. Inferring the mammal tree: Species-level sets of phylogenies for questions in ecology, evolution, and conservation. *PLoS Biol* **17**:e30004941–e30004944.

Van Valen L, 1978. The statistics of variation. *Evol Theor* **4**:33–43.

Verde Arregoitia LD, Fisher DO, Schweizer M, 2017. Morphology captures diet and locomotor types in rodents. *Roy Soc Open Sci* **4**:160957.

Voorhies MR, 1975. A new genus and species of fossil kangaroo rat and its burrow. *J Mammal* **56**:160–176.

Wahlert JH, 1985. Skull morphology and relationships of Geomyoid rodents. *Am Mus Novit* **2812**:1–20.

Weckerly FW, Best TL, 1985. Morphologic variation among rock pocket mice *Chaetodipus intermedius* from New Mexico lava fields. *Southwest Nat* **30**:491.

White J, Downs T, 1961. A new *Geomys* from the Vallecito creek Pleistocene of California, with notes on variation in recent and fossil species. *Contrib Sci* **42**:1–35.

Wilkins KT, Roberts HR, 2007. Comparative analysis of burrow systems of seven species of pocket gophers (Rodentia: Geomyidae). *Southwest Nat* **52**:83–88.

Wilkins KT, Woods CA, 1983. Modes of mastication in pocket gophers. *J Mammal* **64**:636–641.

Wood AE, 1935. Evolution and relationship of the heteromyid rodents with new forms from the tertiary of western North America. *Ann Carnegie Mus* **24**:73–262.

Wyatt MR, Hopkins SSB, Davis EB, 2021. Using 2D dental geometric morphometrics to identify modern *Perognathus* and *Chaetodipus* specimens (Rodentia, Heteromyidae). *J Mammal* **102**:1087–1100.